Cooling System Diagnostics

Author:

David Danielsen

Supervisor:

Ola Stenlåås, Scania

Examiner:

Stefan Grönkvist, KTH

Abstract

To reduce fuel consumption and emissions, engines with higher thermal efficiency and combustion pressure are being developed. Consequently, increased mechanical and thermal stresses may lead to cavitation that may cause cavitation damages on the cylinder liners. Therefore, developing diagnostic methods capable of detecting cavitation events is of interest.

This thesis presents the development of predictive models for detecting cavitation on the cylinder liners, based on the hypothesis that the magnitude of the pressure drop below the saturation pressure of the coolant is proportional to the collapse pressure of vapour bubbles near the liner surface. The model's robustness to varying frequencies of the signal from the pressure measurements at the liners and concentration of glycol was also investigated. Another central part of this study involves analysing the correlation between pressure data collected at a specific system location and the developed model's output based on pressure data measured at the liners, thus enabling the possibility of reliable cavitation diagnostics.

The modelling is based on signals obtained from relative pressure sensors mounted at the liners and an absolute pressure sensor mounted near the system sensor location. Several models were developed using MATLAB and the models were evaluated against a ground truth reference that measures the pressure of the bubble collapses. Initial efforts focused on signal resolution and CPU time conserving calculations. The initial models proved insufficient for predicting cavitation. This led to a more refined approach called the cavitation integral (*CI*) that evaluated the intersection integral between the coolant pressure and the saturation pressure across all analysed engine cycles. Five sub models of the cavitation integral were developed, of which the models *CI 2* and *CI 5* performed the best. None of the models were able to predict the cavitation level with sufficient accuracy. However, the models classified cavitation well when the temperature was constant. *CI 2* and *CI 5* were the objects of a frequency study that illustrated that the models required the bandwidth of the signal to be at least up to 3 000 Hz. Furthermore, both models demonstrated robustness to varying glycol concentration. The correlation analysis was based on the cavitation integral and a negative integral of the system pressure under the baseline pressure. The results demonstrated a weak correlation which resulted in the conclusion that a diagnosis using this method would be insufficient.

In conclusion, the models are capable of classifying whether cavitation occurs or not, but improvements are necessary for the modelling of temperature and flow velocity. However, the pressure difference between the coolant pressure and saturation pressure does not correlate to

the amount of cavitation at the liners. Furthermore, the correlation between system pressure and liner pressure is insufficient to enable a reliable diagnostic of cavitation.

Sammanfattning

För att minska bränsleförbrukningen och utsläppen har länge motorer med högre termisk verkningsgrad och förbränningstryck utvecklats. Detta medför dock ökade mekaniska och termiska belastningar på motorerna, vilket kan leda till kylsystemskavitation och kavitationsskador på cylinderfodren. Något som därför är av intresse är att utveckla diagnostiska modeller som skulle kunna detektera kavitation för att konsekvenserna av ska kunna undvikas.

Det här examensarbetett presenterar utvecklingen av prediktiva modeller för att detektera kavitation runt cylinderfodren i lastbilsmotorer. Modelleringen bygger på hypotesen att storleken ett tryckfall mellan kylvätsketrycket och kylvätskans mättnadsångtryck när ångbildning sker är proportionell kollapstrycket från kavitationsbubblor nära cylinderfodrets yta. Modellernas robusthet undersöktes även med avseende på varierande frekvensinnehåll i trycksignalerna samt olika glykolkoncentrationer I kylvätskan. En annan central del av studien är att analysera korrelationen mellan tryckdata insamlade på en specifik plats i kylsystemet och modellernas utdata baserat på tryckdatan vid fodren. Syftet med detta är att undersöka möjligheten att göra en tillförlitlig kavitationsdiagnos i fordon som är i drift.

Modelleringen baseras på signaler från relativa trycksensorer monterade i kylvätskan nära cylinderfodrena samt en absolut trycksensor monterad nära systemsensorns position. Flera modeller utvecklades I MATLAB och utvärderades mot en referensmodell som mäter trycket från bubbelkollapser. De initiala modellerna fokuserade på signalupplösning och beräkningar som minimerar CPU-tid, men dessa modeller visade sig vara otilräckliga för att detektera kavitation. Detta ledde till en mer avancerad metod, kallad kavitationsintergalen (*CI*), som beräknar skärningsintegralen mellan kylvätsketrycket och mättnadsångtrycket över alla analyserade motorcykler. Fem delmodeller av kavitationsintegralen utvecklades, där *CI 2* och *CI 5* gav bäst resultat. Ingen av modellerna kunde dock förutsäga kavitationsnivån med tillräcklig noggranhet. Däremot fungerade modellerna väl för att klassificera om kavitation förekommer eller inte när temperaturen var konstant. *CI 5* och *CI 2* analyserades vidare i en frekvensstudie, som visade att modellerna kräver en signalbandbredd på åtminstånde 3 000 Hz. Båda modellerna visade även robusthet när glykolkoncentrationen varierades. Korrelationsanalysen baserades på kavitationsintegralen samt en liknande negativ integral av trycket vid systemsensor positionen. Resultat visade en svag korrelation, vilket ledde till slutsatsen att en diagnos som är baserad på denna metod inte är tillräckligt tillförlitlig.

Sammanfattningsvis kan de framtagna modellerna avgöra om kavitation uppstår eller inte, men vidare skulle förbättringar krävas gällande temperatur och flödeshastighet. Resultatet visar även att tryckskillnaden mellan kylvätsketrycket och mättnadsångtrycket inte korellerar med mängden kavitation vid cylinderfodren. Dessutom är kopplingen mellan dessa tryck för svag för att möjliggöra en robust och tillförlitlig kavitationsdiagnostik.

Acknowledgements

I would like to express my sincere gratitude to my supervisor at Scania, Ola Stenlåås, for his valuable guidance, constructive feedback and continuous support throughout my thesis work. I would also like to thank Per Freiholtz, Linus Johansson and Stig Hildahl at Scania for your mentorship, technical insights and collaboration during this thesis.

I would also like to thank my academic supervisor, Stefan Grönkvist, for his support, guidance and constructive feedback during this thesis.

Finally, I am grateful to all the co-workers at Scania whom I have been in contact with, for their helpfulness, expertise and willingness to share knowledge throughout this project.

Table of Contents

0. Definitions

This of section introduces and explains key concepts and terms used throughout this report. The purpose of this section is to provide clear definitions and specify how the terms are used within this thesis, ensuring consistent understanding of each definition throughout the report.

Absolute pressure sensor

A pressure sensor measuring the absolute pressure. The mean value of the pressure measured by the absolute pressure sensor serves as a basis for the baseline pressure modelling.

Bandwidth

Bandwidth refers to the range of frequencies within a signal. In this project the bandwidth is considered to be half the sampling frequency according to the Nykvist criterion or the width of the frequencies specified in a frequency filter used.

Cavitation

Cavitation is the formation and collapse of vapour bubbles in a liquid when the local pressure within parts of the liquid falls below the saturation pressure of the liquid. This phenomenon generates high pressure shock waves and can cause damage on surrounding materials.

Cavitation damage

The damage or potential damage caused by the cavitation phenomenon.

Cavitation models

Cavitation models are the calculation models used within this project with the aim to classify if cavitation occurs and estimate the amount of cavitation.

Crank angle

Crank angle is the rotational position of the engines crank shaft. Within this report the crank angle is defined in degrees. The crank angle vectors in this project ranges from -360° to 360° and resets again. Where 0° corresponds to top dead centre (TDC), see below.

Criterion for cavitation

The "criterion for cavitation" refers to the criterion for vapour formation, which in the context of this report is when the pressure in the coolant decreases below the coolant saturation pressure.

This criterion will be a base for the modelling of this study as its fulfilment is interpreted as the occurrence of cavitation. This criterion is often referred to as “cavitation threshold” throughout the report.

Engine cycle

An engine cycle consists of a sequence of events that in an internal combustion engine convert fuel to mechanical work. For a four stroke engine the sequence of events consists of intake, compression, power and exhaust. During the different steps the piston moves up and down within the cylinder. One engine cycle for a four stroke engine consists of 720 crank angle degrees or two revolutions.

Engine speed

Engine speed refers to the rotational speed of the engines crankshaft. Engine speed is measured in revolutions per minute (RPM) and indicates how fast the engine is operating and is directly related to the motion of the piston.

False negative

For a classification model, a false negative occurs when the model incorrectly predicts a negative case.

False positive

For a classification model, a false positive occurs when the model incorrectly predicts a positive case.

Frequency content

Frequency content refers to the distribution of signal amplitude or energy across different frequencies within a signal. The frequency content indicates the frequencies present, which provides insights into the dynamic behaviour of a system.

Ground truth reference

The “ground truth reference” or the “ground truth method” refers to the modelling approach that establishes the true or expected value of cavitation, against which the other models are evaluated against. The ground truth reference in this project is a model based on high frequency measurements of the bubble collapse and are therefore considered to be the true value of cavitation.

Integral threshold

Integral threshold or threshold level refers to a threshold level used in the modelling of this project where an additional threshold level is introduced to ensure that only engine cycles with a significant amount of cavitation is used to determine if cavitation occurs or not.

Load

Load or engine load refers to the amount of mechanical demand placed on an engine and indicated the amount of work the engine must produce to overcome external resistance. Engine load can be expressed as torque or fraction of the maximum torque that can be produced.

Piston pin offset

Piston pin offset is an intentional lateral displacement of the piston pin. This offset is used for several reasons, one being the reduction of the piston slap and lateral forces on the cylinder walls. The amount of offset of the piston pin can be different for different engines or piston types.

Piston Slap

Piston slap is a mechanical phenomenon that occurs due to the motion of the piston within the cylinder not being perfectly straight. The angle or the connecting rod and the small clearance between the piston and cylinder wall cause the piston to tilt slightly when moving which makes it strike the cylinder wall when changing direction. The strike to the cylinder wall causes the sound called piston slap.

Proximity sensor

Proximity sensor refers to the sensors mounted in coolant at the liners of cylinder 5 and 6 in the context of the correlation analysis made when comparing to the system sensor.

Remote sensor

Remote sensor refers to the system sensor in the context of the correlation analysis.

Sampling Frequency and Nykvist criterion

Sampling frequency refers to the rate at which a continuous signal is measured and converted into discrete values. According to the Nykvist criterion, the sampling frequency must be at least twice the highest frequency present in the signal to capture all the frequency components.

Saturation pressure

Saturation pressure is the pressure where a liquid is in equilibrium with its vapour at a given temperature. At this pressure the liquid begins to vaporise, or the vapour condenses. The saturation pressure for a given temperature can be regarded as the pressure threshold for when cavitation occurs, if the pressure drops below this level bubble formation starts. Throughout the report, the saturation pressure is often referred to as Saturation threshold level or cavitation threshold level.

Saturation pressure threshold

In this report the saturation pressure threshold refers to the physical threshold for cavitation which is the saturation pressure at a given temperature.

Secondary motion of piston

Secondary motion of the piston refers to motions of the piston caused by the connecting rod geometry that deviates from the primary up- and- down motion. Secondary motion of the piston causes phenomenon such as piston slap and vibrations of the cylinder liners.

System pressure

System pressure refers to the pressure level in the expansion tank, which is calculated from the measured pressure from the system sensor.

System temperature

The system temperature refers to the temperature in the coolant measured by the system sensor.

System sensor

System sensor refers to a sensor measuring pressure and temperature in the cooling system and the sensor is located in the outlet channel from the cylinders.

Top dead centre (TDC)

Top dead centre is the position of the piston at the very top of its stroke in the cylinder. Each engine cycle consists of two top dead centres: one at the end of the compression stroke and one at the end of the exhaust stroke. In this report, unless specified, top dead centre refers to the position at 0° crank angle at the end of the compression stroke.

Trigger level

In this project a trigger level is introduced in the modelling part. The purpose of the trigger is to serve as an additional cavitation threshold to the saturation pressure threshold to ensure that only cases with significant amount of cavitation is considered and also to supress background noise that could disturb the modelling.

True negative

For a classification model, a true negative occurs when the model correctly predicts a negative case.

True positive

For a classification model, a true positive occurs when the model correctly predicts a positive case.

Zero pressure level

Baseline pressure level, Zero pressure level or zero level refers to the reference point of the relative pressure sensor signals used in this project. It serves as the baseline from which all pressure variations are measured. This level is set in different ways throughout the development of the models presented in this report. The details of the modelling of the zero pressure level is further explained in chapter 4.

1. Introduction

Greenhouse gas emissions are one the biggest challenges for the automotive industry. To reduce fuel consumption and emissions, engines with higher thermal efficiency are being developed and one way to improve the thermal efficiency is through a higher pressure ratio in the cycle. As a result, this entails greater mechanical and thermal stresses, especially on the cylinder liner, where high pressure fluctuations can induce bubble formation in the coolant known as cavitation bubbles. The cavitation bubbles can cause erosion and damage to the liner, which affects the engine's lifespan and reliability. Therefore, technical solutions such as advanced materials and optimised coolant chemistry are often required to balance the efficiency and durability of the engine.

In heavy-duty engines, the cylinder liner is a critical component that is a subject to mechanical and thermal stresses during operation. As mentioned above, a resulting phenomenon of these stresses is cavitation, a process in which pressure decrease in the coolant lead to the formation and later collapse of vapour bubbles. When the bubbles collapse against the surface of the cylinder liner, wear is created, which over time results in the formation of pits and eventually holes in the liner. These holes causes the coolant to leak into the cylinders, which results in total engine failure. (1,2)

The problem of cavitation is particularly relevant for heavy-duty engines. Since heavy-duty engines often have wet cylinder liners and are designed to be in operation for a substantially longer period compared to passenger cars, the potential damage on the liners due to cavitation increases. In the engines with wet cylinder liners, vibrations of the cylinder liner creates pressure fluctuations in the coolant flowing around. If these pressure fluctuations cause the coolant pressure to locally decrease beneath the saturation pressure of the coolant, the formation of cavitation bubbles will occur. Cavitation damages can occur anywhere on the cylinder liner where the pressure drops below the saturation pressure, but two places are of typical risk for cavitation damages. The first is on the thrust and anti-thrust sides of the cylinder liner where the secondary motion of the piston due to a phenomenon called piston slap affects the liner vibrations the most. The second place is in the narrow channels where the flow rate increases which leads to a decrease in pressure meaning that these areas are more sensitive for pressure fluctuations that causes pressure to drop below the saturation pressure level. (3)

To avoid cavitation, different design strategies can be implemented. Changes to the mechanical properties of the cylinder liners in order to strengthen the cylinders can be implemented to reduce the vibrations. (1,4,5) Another common measure is to integrate a so-called piston pin offset, which helps reduce the risk of cavitation by minimizing uneven pressure distribution on the liners. (4,6,7). System pressure optimisation can be done to increase the difference between the pressure and the saturation pressure threshold for cavitation (8,9). Widening of the coolant water jacket is another measure to mitigate the risk of cavitation. Other strategies can also be implemented, such as using different compositions of the coolant. (6,8,10)

As presented, cavitation in wet cylinder liners has long been an issue that has been tackled with extensive efforts, such as developing design changes and operating strategies to prevent and mitigate the phenomenon. In parallel with preventive approaches to address the problem, diagnostic methods have also been developed to detect and quantify cavitation damage. In a report by Steck et al. (2006), a high-frequency pressure-based measurement technique that captures the dynamic coolant pressure peaks caused by the cavitation bubble collapse was introduced (3). By using sensors in the vicinity of the bubble collapse, this measurement method captures the pressure of the bubble collapse, additionally the researchers introduces a specific formula to evaluate the intensity of cavitation allowing for early detection and diagnosis of cavitation on the cylinder liners. (3)

It is evident that the local conditions around the cylinder liner, such as vibrations and the resulting pressure waves, are, as previously mentioned, the primary causes of cavitation. Another factor that can also be associated with cavitation is reduced system pressure. As the cooling system is pressurised, a reduction in the baseline pressure in the system makes the system more sensitive to pressure fluctuations. Reduced system pressure can be due to several reasons, one example of a common cause is a gas or liquid leakage. Interestingly, something that is noteworthy to be able to prevent cavitation damages, is to find out if there is any connection between the measurable system pressure with the corresponding local pressure around the cylinder liner. Such a connection would facilitate the detection of cavitation and provide a diagnosis for when cavitation occurs, which would make it easier for drivers and workshop technicians to prevent the damage. A connection between the local and measured parameters could provide signals that indicate under which operating conditions cavitation occurs and then provide the drivers or workshop technicians with information about this. The purpose of this thesis is therefore to develop a model that can predict when there is a risk of cavitation. This could give an insight of the local parameter set at the liners for when there is a risk of bubble formation. Furthermore, the purpose is also to investigate the relationship between the measurable pressure from pressure sensor installed in the engine block and the local coolant pressure at the cylinder liners which could lead to a cavitation diagnosis being made. Possible methods for the diagnosis will also be discussed with the purpose of making it possible for drivers or technicians to avoid cavitation damages.

2. Theoretical Background

Several studies have examined the underlying causes of cavitation in cylinder liners, identifying rapid pressure fluctuations as a key contributing factor. When the pressure at the cylinder liners within the coolant drops below its saturation pressure, vapour bubbles form and later collapse as the pressure recovers, generating high-energy impacts on the liner surface. This cycle leads to material erosion, reducing the durability of engine components. Research has shown that liner vibration, caused by the piston's secondary motion and combustion forces, leads to the fluctuation of the pressure in the coolant system which can contribute to the formation of cavitation bubbles (1,3,4,6,9). Additionally, high flow velocities in the cooling channels around the cylinder accelerates contributes to pressure drop which makes these local areas more prone to cavitation. Narrow cooling passages are extra sensitive due to the increase in velocity and further promotes cavitation (3,8,9). Pressure fluctuations caused by piston slap and variations in the cooling system have also been identified as key factors influencing cavitation formation (3,4,7). Furthermore, thermal variations in both the liner and the coolant nearby impact bubble dynamics and influences the formation and collapse of the bubbles (8,9). The properties of the coolant which includes viscosity, density, and saturation pressure, play a significant role in determining the severity and onset of cavitation (1,4,6,8,10).

To minimize the cavitation, various methods have been explored, including mechanical design improvements, coolant modifications, and pressure control strategies. One approach is the use of piston pin offset, which is the intentional displacement of the piston pin from the centre line of the piston. This reduces the lateral forces on the liner and mitigates the liner vibrations and the pressure fluctuations in the coolant (4,6,7). The strengthening of liner materials, such as using chrome-plated liners, is a measure that can be used to enhance resistance to cavitation and extend the lifespan of the liners (1,4).

Another widely researched method is increasing the width of jacket channels where the coolant flows, which improves flow distribution and prevents pressure drops that lead to cavitation (3,8,9). Modifications to coolant composition, including additives that alter surface tension and boiling points, have also been explored to reduce the formation of cavitation bubbles (6,8,10). Additionally, optimizing system pressure is critical in ensuring that pressure levels remain above the saturation pressure threshold, thus preventing bubble formation altogether (8,9).

It is evident that cavitation in wet cylinder liners has been approached both through preventive design strategies and through the development of diagnostic methods aimed at understanding and quantifying the phenomenon. Among these, Steck et al. (2006) introduced a high-frequency pressure-based measurement technique that enables the detection of cavitation by capturing dynamic pressure peaks in the coolant system. (3) These peaks are caused by the collapse of cavitation bubbles and are closely correlated with the severity of potential liner damage. (3)

Cavitation is a complex problem as demonstrated by the many properties and different parts of the cooling system that can be associated to the phenomenon. However, as previously mentioned, the local parameters around the cylinder liner are of particular interest since it is on the cylinder liners that most of the cavitation damage in the cooling system occurs. Numerous reports have in recent years presented attempts to investigate the properties around the liner and also attempts to suggest actions to reduce cavitation. (3, 5, 8, 11)

Liu et al. (2025) investigated how cylinder liner vibrations and cooling jacket pressure changes affect cavitation in diesel engines. They developed a method to predict cavitation by coupling piston dynamics, liner vibrations, and the acoustic properties of the cooling jacket system. The study demonstrated that liner vibrations can create pressure waves in the coolant, and when these are reflected back from the walls of the cooling jacket, this can amplify the pressure decrease and increase the risk of cavitation. The research found that the coolant pressure, cooling jacket width, and sound wave reflections affect the cavitation appearance. Findings indicate that cavitation can be reduced by optimizing both liner vibrations and the acoustic properties of the cooling jacket. (11)

Another important study was conducted by Liu et al. (2024), where they investigated how thin cooling jackets can amplify pressure fluctuations and thereby increase the risk of cavitation. The study presented a novel method for predicting pressure changes by considering the dynamic properties of the cylinder liner and the acoustic amplification in the cooling jacket. The researchers found that thin cooling jackets significantly lower the threshold for triggering cavitation and that liner vibrations and the acoustic properties of the coolant play a central role in the phenomenon of cavitation. The study highlights that optimising both the mechanical properties of the liner and the acoustic properties of the cooling system can be an effective strategy for reducing cavitation. (5)

From the text above and from the introduction of this report it is evident that cavitation has been addressed both through research focusing on preventing cavitation and mitigate the underlying reasons and through methods aimed at quantifying the phenomenon. As previously mentioned, Steck et al. (2006) contributed to this field by presenting a high-frequency pressure-based method for detecting and quantify the intensity of cavitation through capturing high frequency pressure peaks in the coolant due to bubble collapses. As presented in their report, the intensity of the bubble collapse is closely related to the violence of the collapse and the potential damage on the liners. (3)

The measurements presented by Steck et al. aims to capture the highest positive pressure peaks within a defined crank angle window across multiple engine cycles. The window of interest is generally around ignition top dead centre as the piston slap occurs in this crank angle area. Further each pressure peak is classified and weighted according to its potential to cause damage and with this Steck et al formulates the cavitation intensity factor (KI).

In a subsequent study, Bernhard Steck (2008) conducted a parameter study using this method which investigated how various operating and design parameters influenced cavitation. (8) The research revealed that an increase of coolant pressure reduced cavitation intensity. Further a conclusion from the research was that higher chamber pressure and engine load increases cavitation intensity. Other factors such as engine speed and coolant temperature were also investigated and show less direct impact on cavitation compared to coolant pressure and combustion pressure. Design related factors including different pistons and piston geometry was examined in this study and was found to play a critical role. (8)

The findings developed by Steck et al. (2006) underlines the importance of both operational and design tuning. (3) Further the experimental methodology described by Steck et al. builds a foundation for measuring cavitation intensity which enables for a potential diagnosis and detection of cavitation. (3,8)

Despite advancements in previous research, cavitation remains a complex phenomenon influenced by a combination of thermal, mechanical, and fluid dynamic factors. Continued research is necessary to improve predictive models and develop more effective mitigation strategies. Therefore, in this part of the report the relevant theoretical background will be presented. Mathematical equations that govern the cavitation phenomenon will be presented and explained. The initiation, growth and collapse of a cavitation bubble will be introduced and the causes behind cavitation on the cylinder liner along with measures to reduce cavitation will be discussed. Relevant coolant properties for this project will be introduced. In addition to topics related to the cavitation phenomenon, this section will also introduce subjects relevant to the project. The statistic equations used for evaluation of the models will be presented and explained and, lastly, a schematic of the cooling system along with a description of the most important parts of the system within the scope of this thesis will be presented.

2.1 Introduction to cavitation in engines

2.1.1 Fundamental principles and phenomena

Cavitation is a local phenomenon where vapour bubbles form in a liquid when the pressure locally at any given location in the liquid decreases below the liquid's saturation pressure. These bubbles can collapse violently when they encounter higher pressure, leading to high-energy shock waves. (3) In cylinder liners of heavy-duty engines, cavitation is primarily due to pressure fluctuations in the coolant system, which, when it drops below the saturation pressure, initiates bubble formation. (3,9) The understanding of the fundamental thermodynamical principles of cavitation, including the relationship between pressure and vaporisation, is crucial for predicting and mitigating its effects. Cavitation and boiling are similar in that they both consist of vapour formation. However, the two differ in that cavitation is vapour formation due to a drop in pressure while boiling is vapour formation resulting from a rise in temperature. (6)

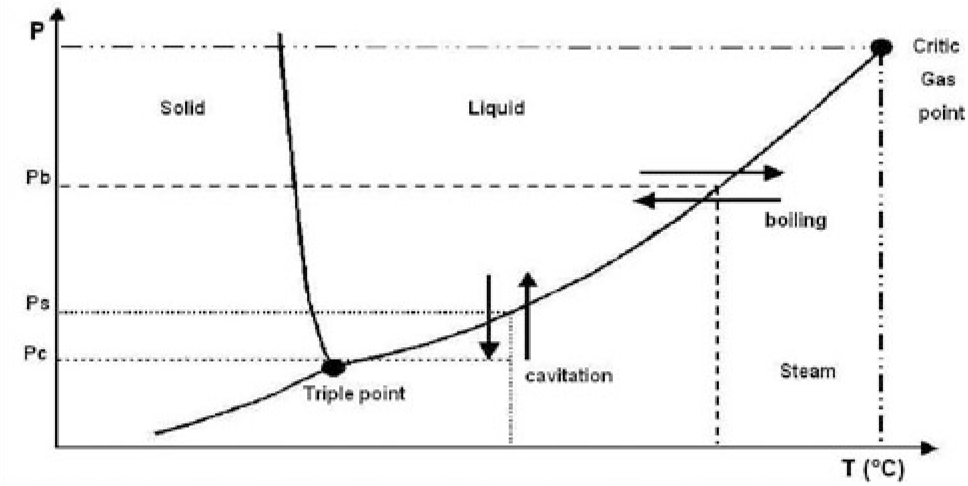

Figure 1: Illustration of cavitation and boiling in a vapour pressure diagram. (6)

Figure 1 illustrates cavitation and boiling in comparison with the saturation pressure of the liquid. The arrows on the left illustrate cavitation meanwhile the arrows on the right illustrate boiling. The requirement for cavitation, as can be seen from Figure 1, is for the local pressure in a portion of a liquid to drop below the saturation pressure. When the pressure then rises, these formed vapour bubbles will transition to the liquid phase again by imploding. In a heavy-duty engine, this formation and collapse of cavitation bubbles is caused by rapid pressure changes in the coolant and is the cause of the erosion that can occur on cylinder liners if this cavitation continues over time. (1,3,4)

2.1.2 Causes of cavitation on the cylinder liner

Cavitation is a complex phenomenon that is caused by many different factors. The factors can be divided into two main groups. The first group is operational parameters as engine speed and load, coolant system pressure, temperature and flow rate, chemical composition of the coolant, cylinder pressure curve characteristic and peak cylinder pressure. While the other group is the design parameters of the piston, the cylinder liners, the cooling channels and the engine block. (8) This section explores the factors leading to cavitation on cylinder liners and its impact on material structures and engine performance.

Cavitation occurs on cylinder liners due to rapid pressure fluctuations caused by piston slap, combustion forces, and coolant flow dynamics. It typically occurs at areas where the pressure fluctuates the most, which are at the thrust and anti-thrust sides of the liner (3,7) and in small passages in the water jacket when the static pressure is low. (3) This is due to the Venturi effect, where increased velocity leads to an equal decrease of the pressure. (1,3,8)

Cavitation damage on cylinder liners is mainly caused by pressure fluctuations resulting from piston slap, liner vibrations, and combustion forces. The piston slap and the liner vibrations is due to the harsh environment that the cylinders operate at, which include high thermal load and mechanical impacts. (5) These vibrations from the piston motion induce rapid pressure drops in the coolant, leading to vapour bubble formation. Additionally abrupt changes in flow properties can further intensifies local pressure drops. (3,6,7)

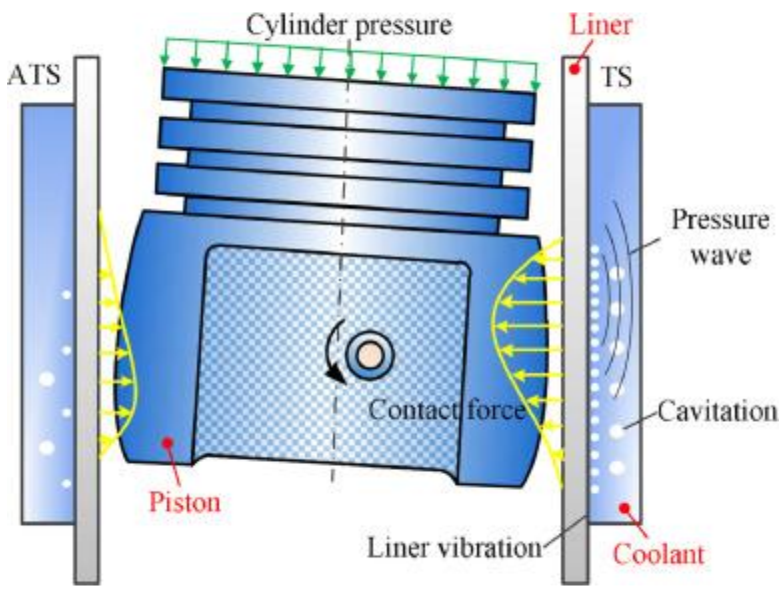

Figure 2: Schematic of liner cavitation due to piston slap (5).

Other factors that influence cavitation are pump velocity, temperature, baseline pressure in the system, engine speed, engine load, impurities in the coolant, coolant composition and dissolved gases in the coolant. The baseline system pressure is an interesting factor that can contribute to cavitation. lowered baseline pressure, increases cavitation risk as the saturation pressure threshold is more easily reached. The presence of a nuclei such as impurities or dissolved gases in the coolant can also facilitate bubble nucleation, enhancing cavitation potential. (3,8)

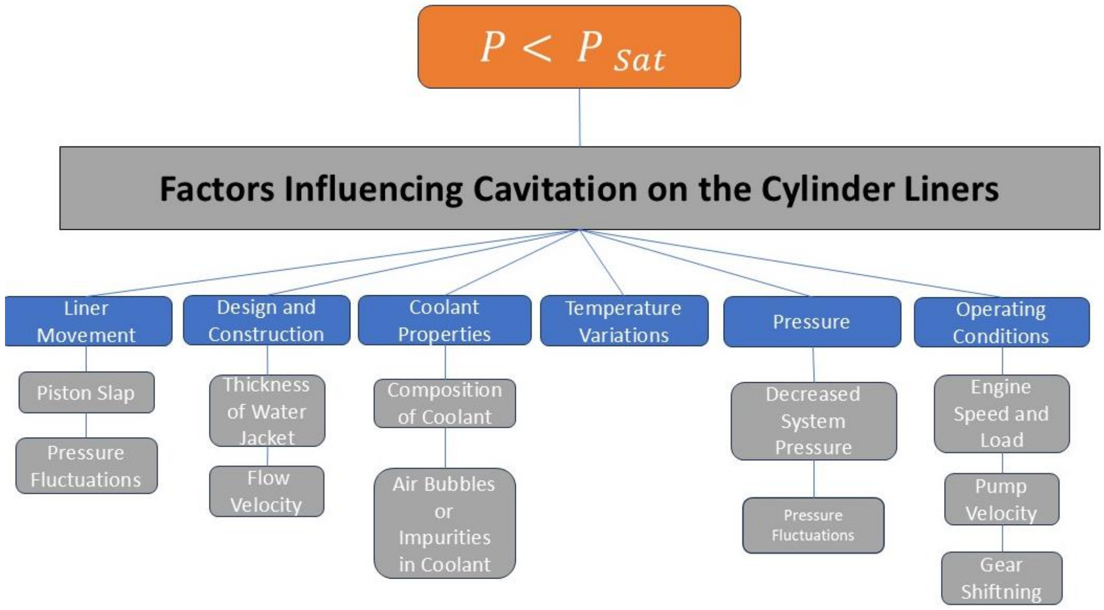

Figure 3: A brief overview of the factors and causes influencing cavitation on the cylinder liners. The image was created by the author and inspired by a figure created by Dr. Ola Stenlåås through personal communication, (2025-03-09). The figure is also made with inspiration from articles that goes through the factors influencing cavitation on the cylinder liners. (1–13)

Figure 3 gives an overview of the factors that can influence cavitation on the cylinder. As illustrated from the figure the problem of cavitation is complex with many interdependent factors. However, the central part of cavitation is that the pressure in the coolant decreases below the saturation pressure threshold. In the picture, this criterion can be illustrated by the fact that all of the factors are linked to the orange box.

2.1.3 Bernoulli's equation for flowing liquids

As previously mentioned, cavitation can occur anywhere on the cylinder liner where the pressure drops below the saturation pressure. Based on Bernoulli's equation for flowing liquids, the effect of the coolant pressure on cavitation can be described. Equation 1, Bernoulli's equation, describes that the total pressure in a flowing liquid is constant. (3,6)

$$P_d = P_{tot} - P_{st} = \frac{1}{2}\rho v^2 \tag{1}$$

Where P_d is the dynamic pressure in the coolant, P_{tot} is the total pressure in the coolant, P_{st} is the static pressure of the coolant, ρ is the density and v is the velocity of the flow.

This means that when the velocity increases, in for example, narrow passages, the static pressure will decrease and if the static pressure decreases below the saturation pressure of the coolant, cavitation bubbles will form. (3,6,8)

2.1.4 Measurements of the bubble implosion and Cavitation Intensity Factor

In their report, Steck et al. (2006) present a method for quantifying the cavitation intensity on wet cylinder liners of heavy-duty diesel engines through the so-called cavitation intensity factor (KI factor). This factor is based on the analysis of high-frequency dynamic pressure peaks in the coolant, which are generated by imploding cavitation bubbles. By measuring and evaluating these pressure peaks, one can gain insight of how severe the cavitation is and predict potential damage to the cylinder liner. (3)

Steck et al. describe that the KI factor is determined by analysing several engine cycles, where the number of cycles varies depending on the engine operating conditions. In transient engine conditions, 50 cycles are usually used, while measurements during steady-state operation may require up to 200 cycles. Regardless of the number of cycles, the KI factor is always normalized to 200 cycles to enable comparisons between different measurements. (3)

When calculating the KI factor, the highest positive pressure peak within a specific crank angle range is identified; it is usually around the ignition top dead centre where liner vibrations are the greatest. These pressure peaks are divided into different intervals and weighted based on their potential ability to cause cavitation-related erosion. The weighted pressure events are then summed and divided by the total number of four-stroke cycles analysed, which provides a measure of cavitation intensity. (3) This method allows engine developers to identify factors contributing to cavitation early and take measures to reduce the risk of erosion and damage to the cylinder liner. The cavitation intensity factor is described by Equation 2:

$$KI = 200\frac{\sum_{k=0}^{m} n_k \cdot f_k}{c} \tag{2}$$

Where KI is the cavitation intensity factor for one KI-cycle, n_k is the number of classified events per section, f_k is the weighting factor, c is the number of measures four stroke cycles, k is the section number and m is the max number of sections.

2.1.5 Cavitation number

To know if cavitation bubbles are formed, a unitless cavitation number is introduced that relates to Bernoulli's equation. (3)

$$\sigma = \frac{P_{st} - P_{sat}}{\frac{1}{2}\rho v^2} \tag{3}$$

Equation 3 describes the cavitation number. Where σ is the cavitation number, P_{st} is the static pressure of the coolant, P_{sat} is the saturation pressure of the coolant v is the velocity of the flow and ρ is the density. The cavitation number relates the pressure in the coolant to cavitation, which occurs when the cavitation number is negative i.e. when the pressure for the fluid is below the saturation pressure. (3,8,12)

2.2 Bubble dynamics

Understanding the dynamics of a cavitation bubble is important to understand what promotes the bubble growth and how the collapse of the bubble impacts and damages the cylinder liner. By analysing the mechanism, it becomes easier to predict and control the conditions that lead to cavitation. Therefore, in this section, the process of bubble growth, bubble collapse and the bubble dynamics close to vibrating and curved surfaces will be introduced and illustrated.

2.2.1 Growth and collapse of a cavitation bubble

The dynamics of cavitation bubbles involve rapid growth when pressure decreases below the saturation pressure, followed by violent collapse as pressure rises again. This collapse generates high pressure shock waves called micro-jets that impact cylinder surfaces and leads to damages. The magnitude of the impact depends on bubble size, collapse velocity, and distance to the surface of the liners. (3,4) The distance between the wall and the bubble is the reason why a thicker coolant jacket led to less damage. (13)

For a bubble to grow, it is crucial that the pressure in the liquid drops, which initiates bubble growth. When the pressure finally becomes low enough to reach the saturations pressure, cavitation bubble formation starts. In an ideal solution without impurities or dissolved gas, vapour formation occurs at this saturations pressure threshold. In real liquids, where impurities or dissolved gases are present, bubble growth can occur even before the pressure threshold is reached. The dissolved gases and impurities are called nuclei and is necessary for the bubble growth to start. (3) Further, implosions of the bubbles happen when the pressure is increased again. The bubble can implode in different ways depending on the surrounding environment. A bubble imploding in an infinite liquid environment will implode symmetrically, as the forces from all directions are equal. However, if a bubble is close to a solid surface, the implosion will be non-symmetrically, creating a so called microjet. The microjets is the reason cylinder liners is subjected to high pressure shocks and damage over time. (3)

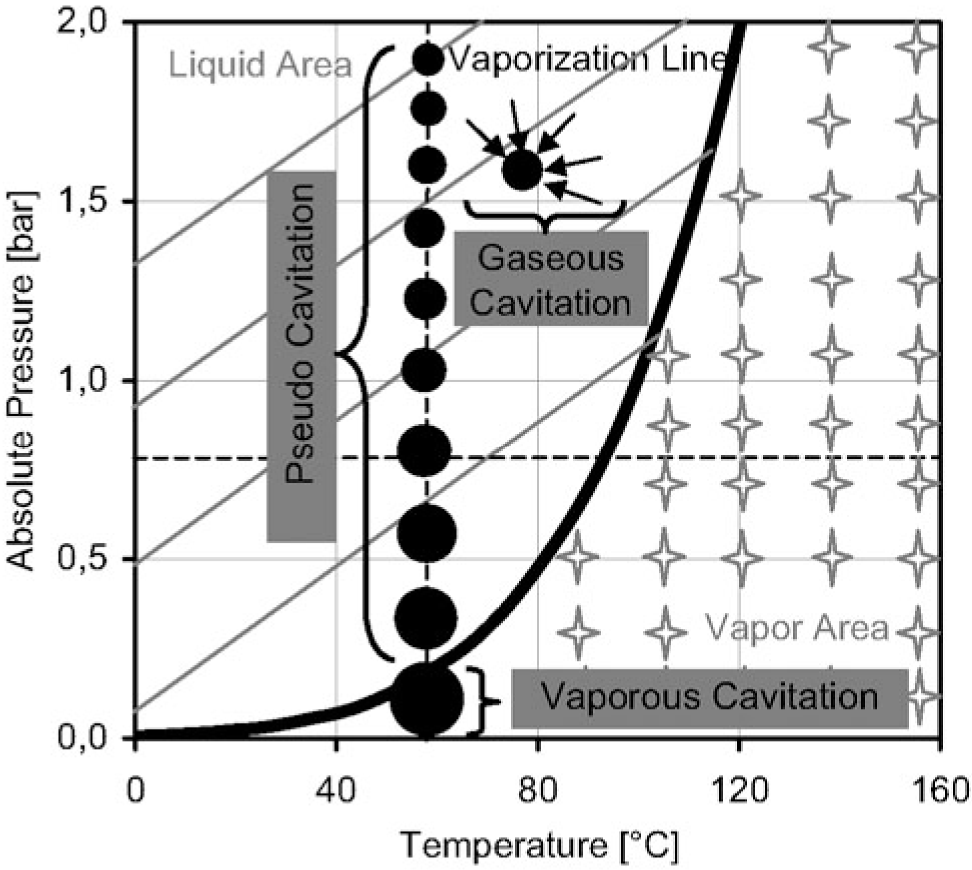

Figure 4: Different types of cavitation. (3)

Figure 4 illustrates the different phases of the bubble growth and the different types of cavitation. (3)

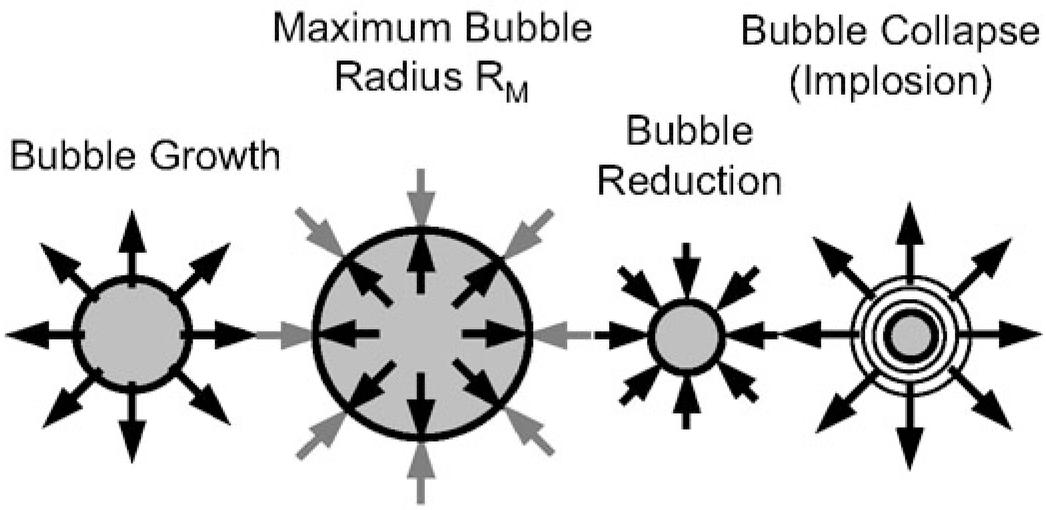

Figure 5: Spherical bubble growth and collapse. (3)

Figure 5 illustrates the spherical growth and collapse of a cavitation bubble in an infinite liquid environment.

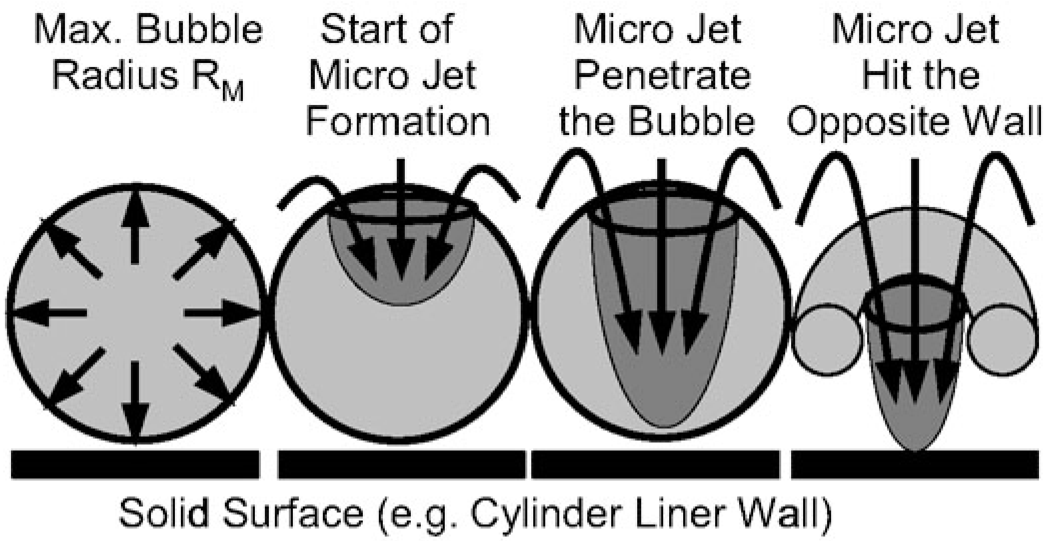

Figure 6: Nonspherical collapse of a cavitation bubble and the formation of a microjet. (3)

Figure 6 illustrates non spherical collapse of a cavitation bubble and the resulting microjet which contributes to the cavitation damage. (3)

2.2.2 Displacement parameter

To determine whether an implosion of a cavitation bubble causes damage to the cylinder wall, the displacement parameter can be used. (3) The displacement parameter relates the distance from the bubble to the wall and whether the bubble will damage the wall. (3)

$$\gamma = \frac{S}{R_M} \quad (4)$$

In Equation 4, γ is the displacement parameter, S is the distance of the centre of the cavitation bubble to the wall and R_M is the maximum bubble radius (3). Steck et al. (2006) claims that cavitation damage occurs when the displacement parameter is less than two. (3)

2.2.3 A cavitation bubble near a cylindrical surface

As mentioned in the previous chapter the growth and collapse of a cavitation bubble is caused by pressure fluctuations and are the reason to the cavitation damage that can be observed on the cylinder liners. However, the dynamics of a cavitation bubble near a solid boundary depends on the geometry and the available space near the boundary. This section presents a short overview of the dynamics of a cavitation bubble near a cylindrical surface.

Cavitation bubbles near cylindrical surfaces displays complex dynamics that differ from those observed near flat boundaries. The interaction between the bubble and the curved geometry gives unique bubble behaviour.

Shen et al. (2025) explored the dynamics of bubbles in confined spaces, comparing flat walls and cylindrical surfaces. Their experiments and theoretical models based on the Kelvin impulse theory, i.e. the intensity of the impulse caused by change into the bubble's movement, showed that the bubble centroid's movement and interface motion could be effectively predicted. They found that the influence of a flat wall on the liquid velocity field is significantly greater than that of a cylinder. Additionally, as the distance between the bubble and the cylinder increases, the velocity of the bubble interface decreases during collapse. (14)

In another study, Shen et al. (2024) examined bubble dynamics near a cylinder within a confined space. They found that bubble collapse behaviours vary depending on the bubble-cylinder distance and radius ratio. The study highlighted three collapse patterns: fan-shaped, ellipse-shaped, and quasi-circular collapses. The Kelvin impulse was observed to decrease exponentially with increasing distance between the bubble and the cylinder, correlating well with experimental observations of jet velocities. (15)

The dynamics of cavitation bubbles near cylindrical surfaces are influenced by factors such as curvature, confinement, and surface characteristics. It is important to know that these interactions influence cavitation and that they should be kept in mind when developing effective mitigation strategies in engineering applications.

2.2.4 A cavitation bubble near a vibrating surface

As the liner vibration is a direct cause of cavitation it is important to study the behaviour of a cavitation bubble near an oscillating surface. The dynamic behaviour of a cavitation bubble near an oscillating surface is significantly influenced by the oscillation parameters, such as, amplitude, frequency, and phase. This section presents a short overview of the dynamics of a cavitation bubble near a vibrating surface.

Zhang et al. (2023) investigated the behaviour of oscillating cavitation bubbles within a narrow gap, which the gap in the cooling jackets may be interpreted as. Their study revealed that both the amplitude of the bubbles oscillation and the frequency affect the acoustic dampening characteristics. The study demonstrated that higher amplitude of the oscillation lead to increased deformation and a change in the dynamics of the collapse of the bubble. The difference in the bubble-wall acceleration and bubble movement was more than 50% compared to bubbles in infinite liquid environments. (16)

For static simulations when all the operating parameters are constant one can assume that in an ideal case the oscillation of the cylinder liners will be constant and have regular phases in the oscillation. For these scenarios there are relationships describing the bubble dynamics near such surfaces. Nguyen et al. (2023) explored the effects of an oscillating curved wall on bubble collapse behaviour through both experimental and numerical methods. Their findings indicated that the phase of wall oscillation plays a crucial role in determining bubble shape, jet formation, and pressure distribution on the surface. In-phase oscillations tend to enhance the collapse intensity and jet velocity, while out-of-phase oscillations can mitigate these effects, reducing potential erosion risks. (17)

These factors influence the bubble dynamics in different ways. Here it is also important to remember these factors when developing engineered strategies to mitigate the cavitation phenomenon.

2.3 Coolant properties

The physical and chemical properties of the coolant, such as viscosity, density, and saturation pressure, play a significant role in cavitation. The saturation pressure of the coolants within the scope of this project is dependent on the fraction of ethylene glycol. For calculation of the saturation pressure Antoine's Equation will be used. Antoine coefficients for a coolant composition of 50 wt.% and 0 wt.% ethylene glycol will be used, and linear interpolation and extrapolation will be applied when necessary. Equation 5 illustrates the version of Antoine's equation that will be used in the modelling part of this project. (18)

$$log_{10}P_{sat} = \frac{A-B}{T+C} \tag{5}$$

Table 1 shows the constants A, B and C used in Equation 5, T is the temperature of the liquid and P_{sat} is the saturation pressure of the liquid. (18)

Table 1: Antoine's constants for water and a mixture of water and ethylene glycol. (18)

Mass percentage of ethylene glycol:	A	B	C
0	7.966820	1668.210	228.000
50	7.901886	1691.452	229.778

Other coolant properties such as viscosity, density, specific heat capacity and Prantl number used in the model development were retrieved from "Technical information Glythermin NF" (2007). (19)

2.4 Cooling system and system sensor location

An important part of this project is to present the cooling system and specify the parts of the system that is important within the scope of this project.

Heated fluid.

Fluid which has passed through a heat consumer, or fluid whose temperature is regulated by mixing cooled and heated fluid.

Cooled fluid

Bleed pipe

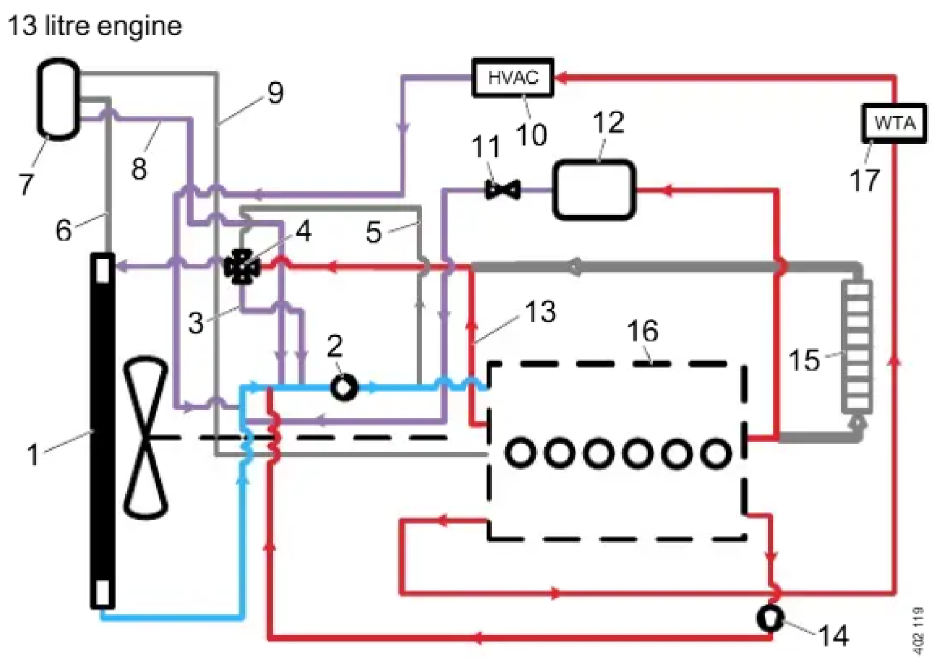

1. Radiator
2. Coolant pump
3. Bypass line
4. Thermostat/Double thermostat
5. Control flow for the double thermostat
6. Radiator bleed pipe
7. Expansion tank
8. Static line pipe
9. Engine bleed pipe
10. HVAC
11. SCR Water valve
12. Reductant tank, SCR
13. Alternative routing when there is no retarder cooler.
14. Air compressor
15. Retarder
16. Engine
17. WTA (Water-to-air)

Figure 7: Flow scheme and components of a cooling system. (20)

Figure 7 illustrates a simple sketch of a cooling system that consists of several important components. The parts that are most relevant to this thesis are the cylinders where the cavitation occurs which are marked with circles in the engine block. The engine block marked as number 16 is another important part, since the cavitation occurs based on the absolute pressure of the engine block and due to the fact that the experimental setup is based on sensors in the engine block. The coolant pump, marked as number 2, is important as it is responsible for increasing the system pressure and allows distinguishing between the pressure in the expansion tank and the pressure in the engine block. Another important part of the system is the outlet pipe, which is the channel that connects the flow from the cylinders to the outlet from the engine block. This pipe is located in the engine block right after the cylinders and is important since the system's pressure and temperature sensor is located there.

2.5 Statistical evaluation metrics

Diagnosis of cavitation in the coolant system is a two folded problem requiring a classification task, i.e. if cavitation occurs, and a problem involving a quantitative estimation, i.e., how much it cavitates. Each calculation model developed in this study can be evaluated against a ground truth model developed by Hubert Herbst at Scania. For each operating case the *ground truth* values can be paired with the corresponding model outputs. This results in two linked data series containing the ground truth value and the model predictions. Based on the two data series, statistical measures and evaluation metrics are used to evaluate the performances of the models. Below, the statistical evaluation metrics $F_1 - Score$ and the coefficient of determination R^2 are defined.

2.5.1 Coefficient of determination R^2

R^2 is a widely used statistical measure to determine the variance in a dependent variable that can be explained by the independent variable in a regression model. This provides information about the fit of a model to a regression line. (21)

In this case R^2 will be used to quantify how well the model output aligns with the ground truth data. However, the pressures of the model and the *ground truth* are interpreted as a physical phenomenon caused by pressure in the system. Therefore, they are of different orders of magnitudes. To facilitate comparison, the ground truth values are mean scaled to the average of each corresponding model output. This simplification enables the analysis to be conducted with respect to the identity line: $model\ output = ground\ truth_{\ scaled}$. The equation used to calculate of R^2 presented in Equation 6 below. (22)

$$R^2 = 1 - \frac{\Sigma\,(y_i - \hat{y}_i)^2}{\Sigma(y_i - \bar{y})^2} \tag{6}$$

Where the numerator is the sum of square of residuals often written as SS_{res} or SSE, and the denominator is the total sum of squares and is often written as SS_{tot} or SST. y_i are the observed values, i.e. the *ground truth* values, $\hat{y}_i$ is the predicted value, which is the model outputs and ȳ is the mean of the *ground truth* values.

The domain of R^2 stretches from negative infinity to 1 and a common interpretation of R^2 is that the parameter compares the mean value of the observed values to the predicted values, which are represented by SSE and SST. If the mean value predicts the observed value better than the model's predictions, then the value can be negative as the residual for the predicted value will be higher than the residual for the mean value. If $R^2$is zero, then the mean value prediction and the model prediction is equally good and if R^2 is between 0 and 1, then the model predicts the observed values better than the mean and the variation in the observed values can then be explained by the model prediction to the extent indicated by the value of R^2. (21–23)

2.5.2 $F_1 - score$ and $F_\beta - score$ for classification of cavitation

For the evaluation of the classification ability $F_1 - score$ will be evaluated for each model. This statistic is the harmonic mean of the recall and precision of the model when the aim of the model is to classify cavitation. (24–26) The classification is based on true positive, false positive and false negative values, where the $F_1 - score$, precision and recall is defined by Equation 7 to 9. (25,26)

$$F_1 - score = 2\frac{Precision \times Recall}{Precision + Recall} \tag{7}$$

$$Precision = \frac{TP}{TP+FP} \tag{8}$$

$$Recall = \frac{TP}{TP+FN} \tag{9}$$

Equation 7 illustrates the $F_1 - score$. The metric is defined as the harmonic mean of precision and recall, which therefore penalize extreme values in either direction. The $F_1 - score$ ranges from 0 to 1, where a higher value indicates a better classification. (25)

To prioritize false positive or false negative points, a weighted version of the $F - score$ can be used. This is called $F_\beta - Score$ and uses the parameter β to weight precision against recall. The β-value is interpreted as how much more important recall is than precision and is specified by the user. (24) Equation 10 illustrates the $F_\beta - Score$. (24,26)

$$F_\beta - score = (1 + \beta^2) + \frac{Precision \times Recall}{\beta^2 \cdot Precision + Recall} \tag{10}$$

The $F_\beta - score$ will be used to optimise settings of the developed model with the aim to prioritize precision and therefore minimize false positive points while still trying to maximize true positive points.

3. Objectives, Delimitations and Research Questions

The main objective of this thesis is to develop a model that predicts cavitation on the cylinder liners and to discuss different methods of how a diagnosis of cavitation can be made based on the correlation between the measurable system pressure and the pressure at the liners. The model will be built using experimental data along with simulation results for verification and comparison of modelling steps. The evaluation of the models will be based on the hypothesis that the difference between that saturation pressure level and the coolant pressure at liners, when the criterion for cavitation is fulfilled, is proportional to the number of bubbles formatted. Therefore, models using pressure differences will be linearly evaluated to the ground truth method that uses the pressure waves from the bubble collapses. To be able to evaluate and visualize this correctly, the pressure when the bubble collapses will be scaled up to the same magnitude as the pressure from the developed models.

To fulfil the aim of this project, the following research questions have been formulated:

- With what accuracy can the developed model predict cavitation on the cylinder liners?
- With what accuracy can the modelled pressure at the cylinder liner correlate to the measured system pressure when cavitation occurs?

However, to narrow the scope of this project, the following delimitations will be made:

- The study will be based on experimental data of the pressure around the cylinder along with temperature, engine properties and properties of the cooling system.
- The pressure sensor at the outlet channel as will be represented by an absolute sensor used in the experiments that this thesis is based on, which is in the vicinity of the system sensor.
- The ground truth method in this study will be based on measurement data of pressure pulses from the bubble collapse.
- Only standard piston pin offset will be considered. Variations in this parameter will not be further investigated.
- Only cooling liquids containing water and ethylene glycol will be considered. Further, the composition of the two compounds will be varied with maximum of 50 percent volume of ethylene glycol. As the composition of the Scania Coolant is a 50 percent volume mixture of ethylene glycol and water. This is because the assumption is that drivers fill up with Scania coolant or clean water, which reduces the volume fraction of glycol. The assumption is based on that some drivers top up with water out of

convenience, while more meticulous drivers use the pre-mixed Scania coolant, which means that the maximum amount of glycol in the system is 50 percent. Another reason is that during this project we may need to induce cavitation, which is made easier in a coolant that consists of more water, as the vapour pressure of water is higher than that of glycol.

- Electrical pumps will not be considered for this model. Only pumps that are dependent on the engine speed will be considered.
- This study will focus exclusively on cavitation on the cylinder liners in the cooling system.

4. Methodology

The aim of the methodology of this thesis is to develop an analytical model to predict cavitation intensity on the cylinder liner based on the local parameters at the cylinder liners, which are pressure, temperature, and flow rate. The aim is also to investigate whether there is any correlation between the coolant pressure at the liners and the measured system pressure when cavitation occurs.

The models will be built in MATLAB through several iterations where different adjustments guided by the hypothesis that the local saturation pressure level is a key factor for the level of cavitation and that the pressure difference when the coolant pressure drops below the saturation pressure is proportional to the number of bubbles formed.

The first iteration models includes using mean values, mean values of negative pressure peaks, and minimum values of the coolant pressure at the cylinder liners. Additional to the various methods for modelling of the pressure at the liners, several methods will be used to determine the saturation pressure level that are used as a criterion for cavitation in the presented models.

The next iteration of the development is to use a pressure signal from the liner that is band pass filtered within the frequencies of 50 to 6 000 Hz. The purpose of the filtration is to capture the fluctuations of the coolant pressure caused by the piston slap and to filter out potential high frequency noise. This signal will be used to capture the pressure fluctuations in the coolant, which can cause cavitation, and a calculation algorithm based on the intersection integral between the coolant pressure at the liners and the saturation pressure threshold will be developed.

The development of the calculation models is based on experimental data provided by Hubert Herbst at Scania. (Personal communication, 2025-03-25) The data was provided as subsets, which was categorised based on system pressure and coolant temperature. The data was split into two sets, where 80% of points was used for development of the models and 20% of the data points for verification of the result. The dataset was split by randomly selecting 20% of the points from each data subset for verification, ensuring that pressure and temperature remained representative between the development set and the verification set.

After each calculation model have been developed, an analysis against the *ground truth* method was carried out using statistics. The models that perform best when comparing to the ground truth method will be analysed using the verification set, which will give insight on the performance of the best models developed in this project. Additionally, results from CFD simulations and 1D simulation provided by Lucas Wernelind (Personal communication, 2025-03-20), Robin Massiquet (Personal Communication, 2025-05-23) and Ahmad Hadadpour (Personal communication, 2025-06-18) at Scania will be used as comparison and verification of modelling steps.

The following part of the methodology will examine in detail the experimental setup used in the experiments conducted by Tommy Andersson at Scania along with the details of the *ground truth* method, the development of models and the details that differentiates the models. This part of the report will also explain the frequency study, simulation of the cavitation integral with different fractions of glycol in the coolant and optimisation of the calculation models that performed the best.

4.1 Modelling of cavitation on cylinder liners

In this part of the report, the methodology of the modelling will be presented. The models include the ground truth reference and the cavitation models developed in this study. The ground truth reference is a model that in similarity with the method presented by Steck et al. (2006) captures the sound of the imploding cavitation bubbles. (3) The calculation models developed in this study includes the models that uses a mean pressure value (*Mean*), which mimics a very slow sensor. Further, models were developed that uses a mean value of the negative pressure samples in relation to the pressure baseline (Def). For this a faster sensor is used to be able to capture the difference between positive and negative pressure when comparing to the pressure baseline. Additionally, it includes models that uses minimum values (*Min*). In similarity to *Def,* a higher frequency sensor will be needed to be able to capture the minimum value of the pressure signal. Lastly, the cavitation integral (*CI*) that uses an intersection integral to calculate the cavitation will be presented. The models are developed using experimental data from experiments conducted by Tommy Andersson at Scania (Personal communication with Hubert Herbst at Scania, 2025-02-06). The experimental setup, the structure of the raw data, and the preprocessing of the raw data will be presented along with the different methods of calculating the saturation pressure level and setting baseline pressure level at the cylinder liners. In section 4.1.7, a summary of each calculation model will be presented.

4.1.1 Experimental setup and structure of raw data

The modelling in this project is based on experimental data, which are from experiments conducted by Tommy Andersson (Personal communication with Hubert Herbst at Scania, 2025-02-06). Andersson used high frequency pressure sensors, which used a sampling frequency of 204 800 Hz, where the bandwidth of the signal is considered to be half of the sampling frequency. The sensors used for the modelling in this project was located in the cooling jacket on the thrust side and anti-thrust sides of the cylinders. (Personal communication with Hubert Herbst at Scania, 2025-02-06)

The sensors relevant for this project are the relative pressure sensors located in the cooling jacket at cylinder 5 and 6 of the test engine. The reason for this is that cylinder 5 and 6 have the piston type that is relevant to the scope of this study. The other sensor relevant for this project is an absolute pressure sensor located in the engine block at the anti-thrust side close to cylinder 4. This sensor is used to set the baseline pressure level for the relative sensors and to represent the system sensors as the two are located close to each other. The relative pressure sensors was Kistler 603B sensors along with a charge amplifier of model PCB 422E03. The absolute pressure sensor is a Keller PAA M5 HB sensor with internal amplifier.

The raw data was time-sampled and was provided as pressure files and crank angle files with the same indexing, meaning that the same index across files correspond to the same time point. This was advantageous as the ignition top dead centre for each engine cycle easily could be found using the crank angle files.

4.1.2 Preprocessing of raw data by extracting and filtering signal

Section 4.1.2 outlines the preprocessing of raw data prior to the modelling.

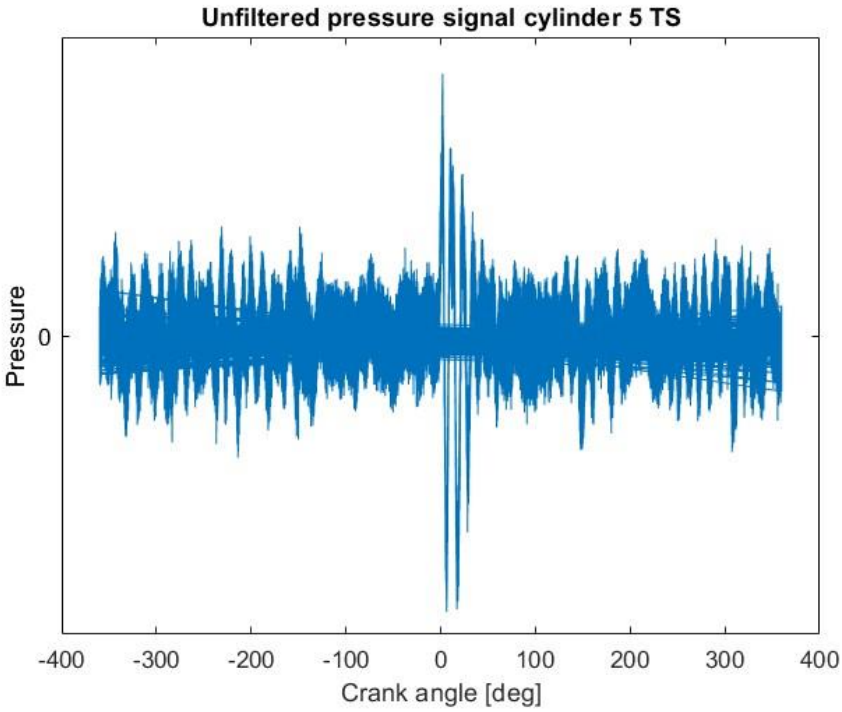

Figure 8: Unfiltered pressure signal from thrust side at cylinder 5 during steady state conditions, 1 800 RPM, 115% load, 90 °C coolant temperature and 1.6 bar of system pressure.

Figure 8 illustrates an unfiltered pressure signal with sampling frequency of 204 800 Hz. The pressure signal is from a relative pressure sensor, where the zero level is the ambient pressure. The signal in Figure 8 is a cavitating case, and the minimum pressure peaks are pressure fluctuations in the coolant close to the cylinder, which are caused by the piston slap. The unfiltered signals are used for the models *Mean*, *Def* and *Min*.

For the *ground truth* model, frequency filters were used to capture the high frequency pressure peaks of the bubble implosions.

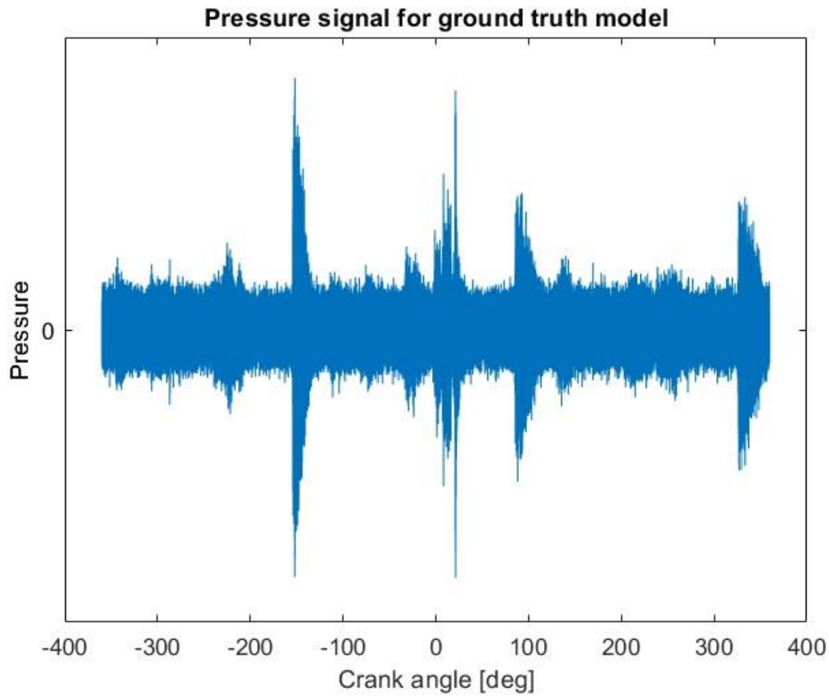

Figure 9: Filtered signal with the purpose of capturing the high frequency bubble collapse. The signal is from the steady state conditions at 1 800 RPM, 115% load, 90 ℃ coolant temperature, and 1.6 bar of system pressure obtained from the sensor mounted at the thrust side of cylinder 5.

Figure 9 illustrates a filtered signal from the relative pressure sensors at the liners which is used to capture the high frequency pressure peaks caused by the bubble collapses. The signal in Figure 9 is a cavitating case, and the minimum pressure peaks and the maximum pressure peaks are caused by the bubble collapses which occurs in the same crank angle region as the piston slap i.e. in a crank angle domain after TDC.

For the *CI* methods, a bandpass filter with limits at 50 Hz and 6 000 Hz was applied to the pressure signals. The purpose of the frequency band in the filtration was to emulate a signal that could be obtained from a sensor installed in a production engine and captures the pressure fluctuations in the coolant caused by the piston slap.

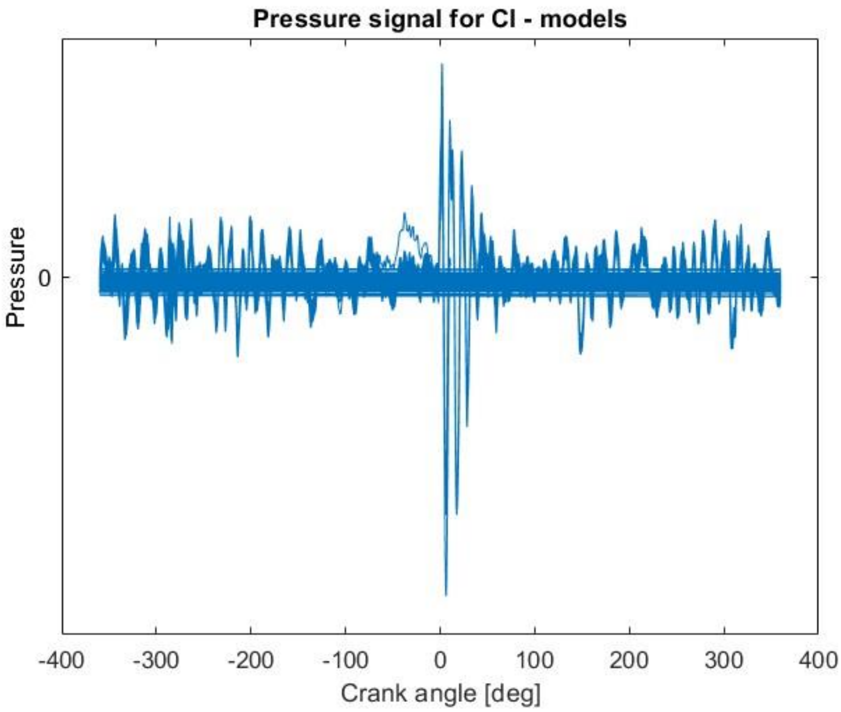

Figure 10: Filtered signal with frequency limits 50 Hz and 6 000 kHz. The signal in this figure is from the steady state conditions at 1 800 RPM, 115% load, 90 ℃ coolant temperature, and 1.6 bar of system pressure obtained from sensor mounted at thrust side of cylinder 5.

Figure 10 illustrates a filtered pressure signal which is used to capture pressure fluctuations caused by piston slap. The signal is from a relative pressure sensor, and the case is a cavitating case. The minimum pressure peak are fluctuations in the coolant close to the cylinder.

4.1.3 Calculating saturation pressure level and baseline pressure level

The models in this project are all based on the coolant pressure at the cylinder liner decreasing below the saturation pressure. One part of the development of the models is to model the saturation pressure of the coolant as well as setting the baseline pressure at the liners as the sensors used for the modelling are relative pressure sensors. This can be done in several different ways under certain assumptions.

To calculate the saturation pressure’s dependence of the temperature, Antoine's equation is used. Additionally, the baseline pressure needs to be set for the saturation pressure to be correct in relation to the coolant pressure.

Below, the different methods to model temperature and baseline pressure are described. These different methods will then be used to create the calculation models.

4.1.3a Temperature modelling

There are two different ways to model the temperature. The first is by using the temperature from the system sensor. The second is by assuming that the interaction of the coolant with the cylinder follows the dynamics of heat transfer around a hot cylinder in a cross-flow with highly turbulent conditions.

By assuming that the coolant flow follows a two dimensional cross-flow around a cylinder, the following modelling of the temperature can be derived. The temperature change around the cylinder was approximated by Equation 11 which describes a local energy balance for convective heat transfer from a cylinder to a passing fluid along the surface in a cross-flow system.

$$\frac{dT}{ds} = \frac{h(\phi)\cdot L}{\dot{m}\cdot C_p}(T_s - T(\phi)) \tag{11}$$

Equation 11 is a differential equation that describes a one-dimensional temperature increase in the circumferential arc length of a cylinder. Where T is the temperature, T_s is the surface temperature, L is the length of the cylinder in axial direction, $\dot{m}$ is the mass flow, C_p is the heat capacity of the coolant, h is the heat transfer coefficient, s is the arc length of the cylinder, and ϕ is the circumferential angle along the cylinder surface starting from the stagnation point and increasing in the direction of the flow. The arc length can be expressed in terms of angle and radius as, $ds = d\phi \times R$. In order to solve this differential equation for the temperature at the end of the cylinder where $\phi = 180°$, the forward Euler method is used in MATLAB with discretized values of h at every tenth degree.

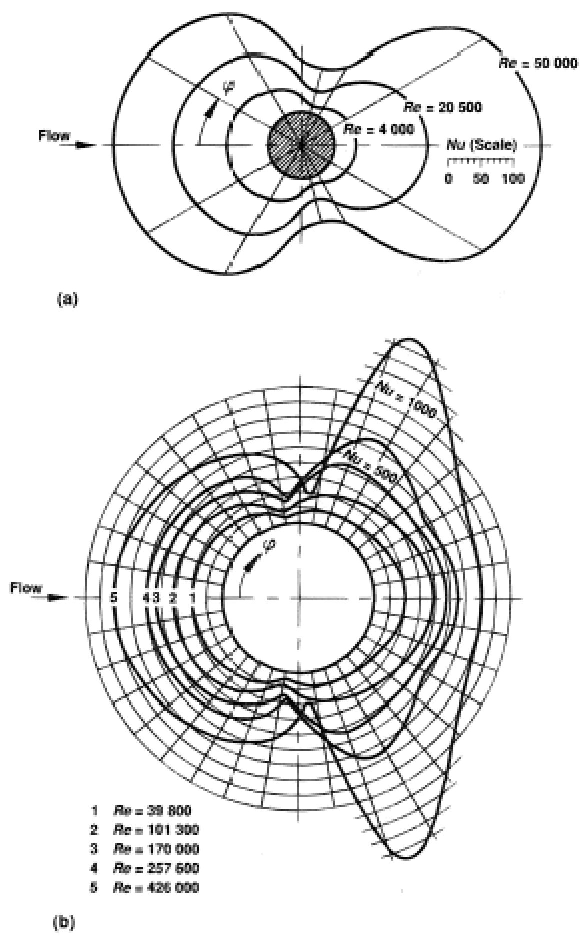

Figure 11: Local Nusselt numbers for air flow around cylinder for different flow regimes. (27,28)

To solve this differential equation, some assumptions are made. The first assumption describes a boundary condition is that the wall temperature T_s has the same temperature as the coolant at the solid-liquid interface. T_s can thus be calculated by Equation 14. Regarding the heat removed from the cylinders to the coolant this quantity is estimated to be half as much as the work through crankshaft. The wall temperature can then be estimated through Equation 12-14, where Equation 14 is a simplified heat transfer equation that describes the heat transfer between the wall temperature and the bulk temperature.

An assumption must be made regarding initial and boundary values to be able to solve the differential equation, this is that the bulk temperature and the initial temperature are assumed to be equal to the system temperature obtained from the system sensor. Another simplification that was applied to the modelling of the temperature was regarding the flow characteristics. It is that the Reynolds numbers in this project was such that the Nusselt numbers for $Re = 426\,000$ obtained from Figure 11 could be used. This assumption is based on calculations of the Reynolds number for a two- dimensional cross flow around a cylinder where the velocity was calculated based on measurements of the cooling channel around the cylinder and the volume rate of coolant into each cylinder. The purpose of this approximation was to reduce the computational complexity while still have a flow dependent model of the temperature.

Another estimate is also done regarding the flow regime, which is that the Reynolds number is in the same flow regime as the Nusselt numbers with Reynolds numbers at 426 000 which allows the use of Nusselt numbers from Figure 11.

Since Figure 11 shows the Nusselt number for air flow around a hot cylinder (27,28), these values must be scaled up using Equation 15 which describes how the Nusselt number depends of the Prantl number (29). Through these assumptions, the local temperature after contact with the cylinder can be found. The following part gives a description of the equations used for the modelling of the temperature.

$$Q_{cool} = 0.5W \tag{12}$$

Equation 12 is used to estimate the heat removed from the engine through the coolant and is estimated to be half as much as the work extracted through the crankshaft which are dependent of the engine torque.

$$Nu_{av} = 0.3 + \frac{0.62\, Re_D^{1/2} Pr^{1/3}}{[1+(\frac{0.4}{\mathrm{Pr}})^{2/3}]^{1/4}} \cdot [1 + (\frac{Re_D}{282000})^{5/8}]^{4/5} \tag{13}$$

Equation 13 is the Bernstein- Churchill equation and provides an empirical expression of the average Nusselt number for forced convection for a crossflow around a cylinder. (30)

$$Nu = \frac{h \cdot L}{k} \tag{14}$$

$$T_s = T_{bulk} + \frac{Q_{cool}/6}{h_D \cdot A_{mantle}} \tag{15}$$

$$Nu = 0.26 Re^{0.6} Pr^{0.3} \tag{16}$$

Equation 14 and 15 is the definition of the Nusselt numbers and the heat transfer from the surface of solid wall to the bulk of the fluid. Equation 16 describes the relation between the Prantl and Nusselt number for forced convection and can be used to scale the values obtained from an air flow to corresponding values for a coolant flow (29).

These estimations and equations are used to model the local temperature after contact with the cylinder. Equation 11-16 creates direct flow rate, engine speed and load dependencies for the temperature which does not exist if temperature from the system sensor is used. However, in cases where the system sensor is used the temperature remains affected by the flow rate and the engine speed as its location is after the coolant pump.

4.1.3b Pressure modelling

To set baseline pressure in the coolant, three different modelling approaches was used. The first was to set the baseline pressure level using the pressure in the expansion tank. The second was to use the mean value of the absolute pressure from the absolute pressure sensor in the engine block and the third was to use pressure coefficients in a cross flow around a cylinder.

4.1.3b(i) Pressure in expansion tank

The first approach uses the pressure in the expansion tank as the baseline pressure level. This approximation is considered acceptable as it reflects the overall system pressure and variations in the degree of pressurization within the system. The shortcomings of this method are rooted in how the cooling system is structured. The expansion tank is located before the pump and therefore does not receive the pressure increase that the pump contributes, which leads to a baseline pressure level that is too low and also independent of the engine speed and pump velocity.

4.1.3b(ii) Pressure from absolute sensor

Another method is to use the mean value of the pressure from the absolute pressure sensor as the baseline pressure level. This sensor is located in the engine block and therefore receives the increased pressure from the pump and the variations that depend on engine speed. This represents a modelling simplification as the pressure sensor is not located in the vicinity of the liners. Nevertheless, when comparing the pressure differences between various regions of the engine block obtained from one- dimensional simulations with the pressure difference between the mean of the pressure from the absolute sensor and the saturation level, this simplification is justified

since the different between different regions of the engine block is relatively small. (Personal communication with Robin Massiquet, 2025-05-23)

4.1.3b(iii) Pressure using pressure coefficient

The last method for modelling of the baseline pressure level is to approximate pressure at the liner by using pressure coefficients in an incompressible flow. (31) In this application the relevant pressure coefficient is for the position behind the cylinder.

$$P = P_{inf} + 0.5 C_P v \rho \tag{17}$$

Equation 17 describes the pressure using pressure coefficients in an incompressible flow, where P is the adjusted pressure relevant to the position in the flow, P_{inf} is the pressure in the inflow to the cylinder, which is approximated as the mean of the pressure from the absolute pressure sensor. ρ is the density of the liquid, v is the velocity in the inflow to the cylinder and C_P is the pressure coefficient for a cross flow around a cylinder at the end of the cylinder, which for the flow regimes relevant for this application is approximated as -1. The approximation of the pressure coefficient was -1 and was done from (32) and (33). The relevant flow regime was approximated trough calculations using experimental data and simulation data. (31)

4.1.3c Summary of pressure and temperature modelling

Through the presented approximations and assumptions in section 4.1.3a and section 4.1.3b, the saturation pressure can be calculated using different methods of modelling temperature along with different methods for modelling the baseline pressure level in the coolant close to the cylinder liners. This creates several different methods for modelling the temperature and pressure which are summarized in Table 2. The models listed below are presented in section 4.1.5 and section 4.1.6. The input data in the table below are the methods of estimating the pressure and temperature at the liners, which are used to model the saturation pressure level and the coolant pressure at the liners. These two parameters are then used to estimate the cavitation.

Table 2: Methods for pressure and temperature modelling for each model and the necessary input data.

Model	**Temperature**	**Pressure**	**Input data**
Mean 1	System sensor	Absolute sensor	Coolant temperature, Absolute pressure
Mean 2	System sensor	Absolute sensor	Coolant temperature, Absolute pressure
Mean 3	Differential equation	Pressure coefficient	Coolant temperature, Absolute pressure, Engine speed, Engine torque
Def 1	System sensor	Absolute sensor	Coolant temperature, Absolute pressure
Def 2	Differential equation	Pressure coefficient	Coolant temperature, Absolute pressure, Engine speed, Engine torque
Min 1	System sensor	Absolute sensor	Coolant temperature, Absolute pressure
Min 2	Differential equation	Pressure coefficient	Coolant temperature, Absolute pressure, Engine speed, Engine torque
CI 1	System sensor	Expansion valve	Coolant temperature, System pressure
CI 2	System sensor	Absolute sensor	Coolant temperature, Absolute pressure

CI 3	System sensor	Pressure coefficient	Coolant temperature, Absolute pressure, Engine speed
CI 4	Differential equation	Pressure coefficient	Coolant temperature, Absolute pressure, Engine speed, Engine torque
CI 5	Differential equation	Pressure coefficient	Coolant temperature, Absolute pressure, Engine speed, Engine torque

4.1.4 Ground truth reference

Another important part to introduce prior to the methodology of the calculation models is the *ground truth reference*. This model is developed by Hubert Herbst at Scania. The *ground truth reference* determines the level of cavitation at the cylinder liners by capturing the sound of the imploding bubbles at the liners which are of high frequency nature. (3) Similarly to the method developed by Steck et al. (2006) which uses high frequency measurements in a crank angle window around the top dead centre, the *ground truth reference* uses high frequency content from the same region at the crank angle axis around TDC to determine the amount of cavitation. (3,8)

The purpose of the *ground truth reference* within the scope of this project is to calculate results that will serve as a reference, against which the performance of the other developed models can be evaluated. The model provides a consistent reliable baseline for cavitation, which provides objective comparison and validation of the predictive accuracy of the other proposed calculation models.

4.1.5 Cavitation level using mean pressure, deficit of pressures and minimum values of pressure

As previously mentioned, the first developed models are based on signal resolution and CPU time conserving calculations that use the unfiltered pressure file to calculate the difference between the saturation vapour pressure and the coolant pressure when the criterion for cavitation is fulfilled. These calculations can be roughly divided into three categories. Mean models (*Mean*), Deficit models (*Def*) and Minimum models (*Min*). What distinguishes the sub-models is how the relative pressure levels are adjusted and how the temperature is estimated.

The mean value models are the simplest for approximating cavitation and use a mean value of the pressure signal. This can be compared to the signal of a slow sensor. The mean value is compared to the saturation pressure and if the liner pressure is below the saturation vapour pressure, it is considered as cavitation. Three different ways of modelling cavitation with a mean value are used, *Mean 1*, *Mean 2* and *Mean 3*. *Mean 1* and *Mean 2* uses the absolute pressure sensor in the engine block to set the baseline pressure level at the liners and the temperature from the system sensor. *Mean 3* uses pressure coefficients to set the baseline pressure level and a differential equation to model the temperature. The difference between *Mean 1* and *Mean 2* is that *Mean 2* uses an offset to adjust the baseline pressure level so that it is closer to the saturation vapour pressure. This is done as an adjustment of *Mean 1* as its values essentially will show no cavitation response due to the cancellation effects of the negative and positive components compared to the baseline pressure level. Initially, the offset is adjusted so that the baseline pressure level is on par with the saturation vapour pressure for several of the analysed cases. This implies that the mean value, for some cases, can be below the saturation level.

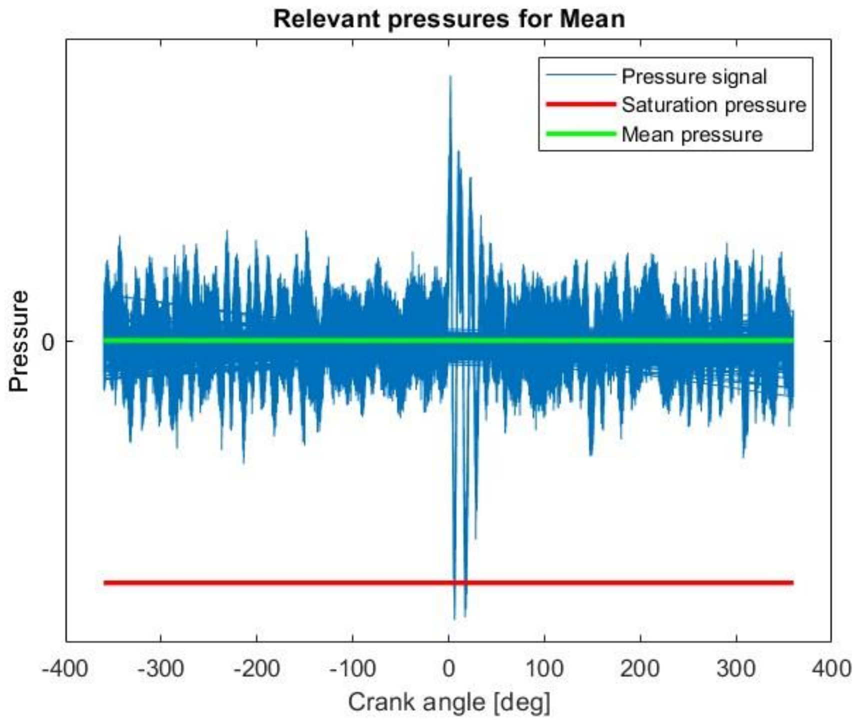

Figure 12: Relevant pressures for *Mean* models. Signal from 1 800 RPM, 115 % load, 1.6 bar system pressure, 90 °C system temperature, cylinder 5 thrust side.

The pressure deficit models (Def) provide a further nuance to the calculations, different from *Mean*. Since it is the negative fluctuations in the coolant pressure at the liner that lead to vapour formation and cavitation, the *Def*- models use a mean value of the pressure components below defined baseline pressure level. An unfiltered signal was used with a sampling frequency of 204 800 Hz. This is necessary because the sensor must be able to distinguish between positive and negative pressures. *Def 1* uses the absolute pressure sensor in the engine block to set the baseline pressure level and temperature from the system sensor and *Def 2* uses pressure coefficients and a differential equation to calculate the temperature.

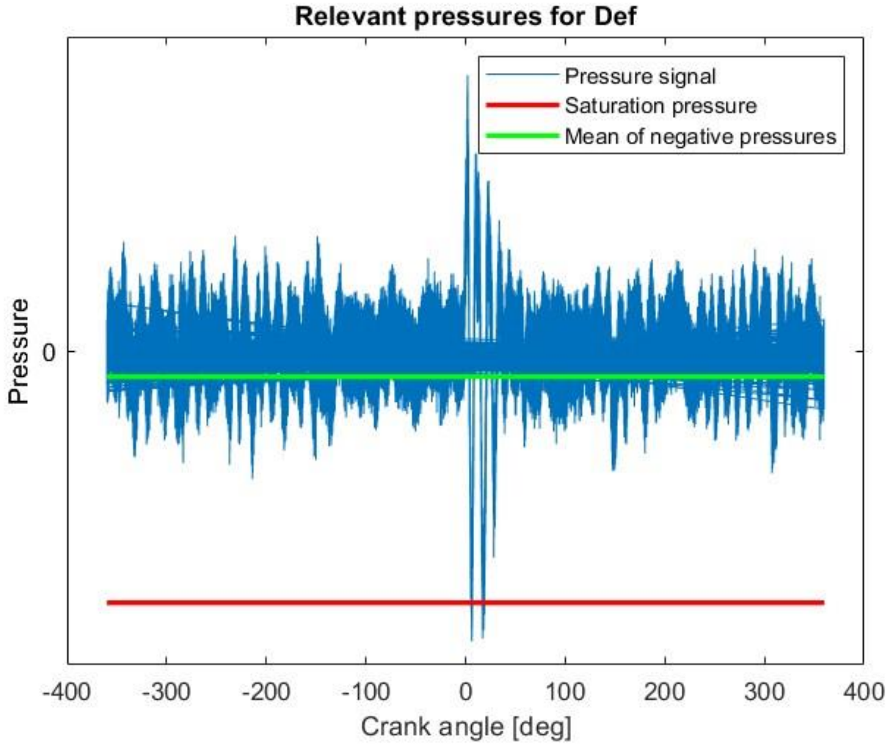

Figure 13: Relevant pressures for *Def* models. Signal from 1 800 RPM, 115 % load, 1.6 bar system pressure, 90 °C system temperature, cylinder 5 thrust side.

Finally, an approach using the minimum value for the evaluation against the saturation pressure is developed (*Min*). The sub-model *Min 1* uses the absolute pressure sensor in the engine block to set the baseline pressure level and the temperature from the system sensor while *Min 2* uses pressure coefficients and a differential equation.

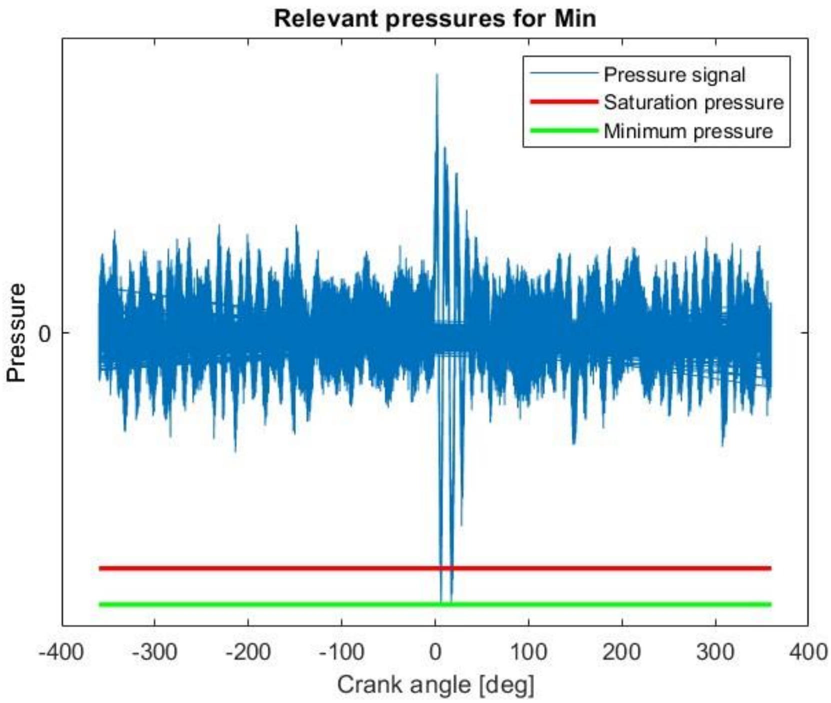

Figure 14: Relevant pressures for *Min* models. Signal from 1 800 RPM, 115 % load, 1.6 bar system pressure, 90 ℃ system temperature, cylinder 5 thrust side.

The model outputs for *Mean Def* and *Min* are evaluated against the *ground truth* values using statistical measures to see if these can be used to classify and predict the amount of cavitation.

4.1.6 Calculation of Cavitation using Cavitation Integral

The cavitation integral (*CI*) is a more complex method for modelling cavitation, and it is based on the previous models *Mean*, *Def* and *Min* but is using a more developed methodology, which is based on the intersection integral between the pressure signal at the cylinder liner and the saturation pressure. During the development of this model, five sub-models were created, which are called *CI 1*, *CI 2*, *CI 3*, *CI 4* and *CI 5*. All sub-models are based on an intersection integral, which is being calculated if the criterion for cavitation is fulfilled. Unlike *Mean, Def* and *Min* which evaluates the pressure during the full engine cycle, the *CI* models focuses their analysis on a targeted crank angle window surrounding TDC with the aim to capture pressure fluctuation in the coolant due to the piston slap. What distinguishes the sub-models are details such as settings, pressure modelling, and temperature modelling. The section below presents a detailed description of the development of the *CI-models*.

As described in section 4.1.2, a signal with a frequency range within 50 – 6 000 Hz is used for the calculations. Further, in each engine cycle, a crank angle axis window of -13° to 34° around the TDC was analysed to include the pressure fluctuations caused by piston slap. In this window, an intersection integral between the saturation pressure and the coolant pressure at the liner is calculated if the criterion for it is satisfied. The integral is set to zero for cases where the criterion for cavitation is no satisfied. The integral is then divided by the length of the crank angle interval of focus, which gives the value of the scaled integral in units of pressure. The interval length is derived from the number of samples present within the specified crank angle window and is dependent on the engine speed. A root mean square value of the integral for each engine cycle is then calculated and is considered as the value of the cavitation integral *CI*. By using the root mean square in instead of an arithmetic mean, engine cycles with significant cavitation are given greater weight. This ensures that the analysis emphasizes cycles with substantial content rather than averaging out meaningful variations. This effect is pronounced only if the signal exhibits considerable variations across motor cycles.

The difference between sub models lies in how the baseline pressure levels are set, how the temperature is modelled and how thresholds are used to adjust the requirement for it to be considered as cavitation. *CI 1* uses the pressure from the expansion tank and the temperature from the system sensor. *CI 2* uses the pressure from the absolute pressure sensor and the temperature from the system sensor. *CI 3* uses the temperature from the system sensor and pressure coefficients to set the pressure level. *CI 4* uses a differential equation to calculate the temperature and pressure coefficients to set the pressure level. *CI 5* uses the same pressures and temperatures as *CI 4* but also adds two cavitation thresholds. The first threshold is a trigger level. It is used as an additional pressure barrier to the saturation level that the liner pressure must fall below in order for the area between the saturation vapour pressure and the liner pressure to be calculated. The second is a threshold for the normalized integral for each engine cycle and operates so that if the normalized integral over a single engine cycle is lower than the defined threshold, its value is set to zero prior to the calculation of the root mean square in the subsequent step. Initially, the trigger level was 40 kPa and the threshold level was 25 kPa. These settings are then selected for *CI 5* and used similarly on *CI 2* in an optimisation of the settings for the two models as the two had the best ability of the models to classify cavitation.

4.1.7 Summary of calculation models

Table 3 illustrates a summary of the developed models the prediction of cavitation. The table presents the model description, the model inputs, the model outputs and evaluation notes of the model.

Table 3: Summary of calculation models.

Model ID	Model description	Input	Output	Evaluation notes
Mean 1	*Mean* value model.	Temperature, pressure, mean of pressure at cylinder liner.	Classification of cavitation and pressure difference between liner pressure and saturation pressure.	Evaluated across entire signal.
Mean 1	Mean value model with offset.	Temperature, pressure, mean of pressure at cylinder liner.	Classification of cavitation and pressure difference between liner pressure and saturation pressure.	Evaluated across entire signal. Offset used.
Mean 3	Mean value model with local parameters.	Temperature, pressure, mean of pressure at cylinder liner.	Classification of cavitation and pressure difference between liner pressure and saturation pressure.	Evaluated across entire signal.
Def 1	Mean value of pressure deficit.	Temperature, pressure, pressure signal from liners with frequency of 204 800 Hz.	Classification of cavitation and pressure difference between liner pressure and saturation pressure.	Evaluated across entire signal.
Def 2	Mean value of pressure deficit with local parameters.	Temperature, pressure, pressure signal from liners with frequency of 204 800 Hz.	Classification of cavitation and pressure difference between liner pressure and saturation pressure.	Evaluated across entire signal.
Min 1	Lowest value	Temperature, pressure, pressure signal from liners with frequency of 204 800 Hz.	Classification of cavitation and pressure difference between liner pressure and saturation pressure.	Evaluated across entire signal.
Min 2	Lowest value with local parameters	Temperature, pressure, pressure signal from liners with frequency of 204 800 Hz.	Classification of cavitation and pressure difference between liner pressure and saturation pressure.	Evaluated across entire signal.
CI 1	*CI* with pressure in expansion tank and temperature from system sensor.	Temperature, pressure, pressure signal from liners with bandpass filter limits at 50–6000 Hz.	Classification of cavitation and root mean value of scaled cavitation integral from specific window on the crank angle axis.	Evaluated over a crank angle window around TDC.*

CI 2	*CI* with absolute pressure and system temperature.	Temperature, pressure, pressure signal from liners with bandpass filter limits at 50–6000 Hz.	Classification of cavitation and root mean value of scaled cavitation integral from specific window on the crank angle axis.	Evaluated over a crank angle window around TDC.*
CI 3	*CI* with local pressure	Temperature, pressure, pressure signal from liners with bandpass filter limits at 50–6000 Hz.	Classification of cavitation and root mean value of scaled cavitation integral from specific window on the crank angle axis.	Evaluated over a crank angle window around TDC.*
CI 4	*CI* with local parameters.	Temperature, pressure, pressure signal from liners with bandpass filter limits at 50–6000 Hz.	Classification of cavitation and root mean value of scaled cavitation integral from specific window on the crank angle axis.	Evaluated over a crank angle window around TDC.*
CI 5	*CI* with local parameters and thresholds.	Temperature, pressure, pressure signal from liners with bandpass filter limits at 50–6000 Hz.	Classification of cavitation and root mean value of scaled cavitation integral from specific window on the crank angle axis.	Evaluated over a crank angle window around TDC.* Threshold used.

*A window from -13 to 34 crank angle degrees was first used, but the window settings was subsequently optimised

4.2 Optimisation of settings

Two optimisations of settings for the models were made, one to optimise the settings *of* the ground truth method and *CI* to get the best classification possible by maximizing the $F_1 - Score$. The other by using F_β with $\beta = 0.2$, which weighs precision more, which, in turn, means that false positives are minimized and true positives are maximized. This will minimize false cavitation alarms and can provide a result on how the model performs under this requirement. *CI 2* and *CI 5* was the models with the highest ability to classify cavitation and are therefore the objects of this optimisation study. In the optimisation, the trigger and threshold levels were also introduced to the optimisation of *CI 2* but were given a starting value of zero to investigate whether these thresholds would contribute to increased classification ability.

In this optimisation study, MATLAB's pattern search function was used, which means that the optimisation is derivative-free and uses a grid of points to find a local minimum. This function is particularly useful where gradient information is missing, difficult or time-consuming to calculate. The algorithm is based on searching for solutions in a grid and then adjusting this grid dynamically based on the best solution. The function works in both cases with linear and non-linear constraints. The following options were used in the optimisation for this project. (34)

```
options = optimoptions('patternsearch', ...
    'Display', 'iter', ...
    'UseCompletePoll', true, ...
    'UseParallel', false, ...
    'MaxIterations', 300, ...
    'MeshTolerance', 1e-4);
```

Figure 15: Settings used for optimisation.

Since pattern search is a local optimisation algorithm, different starting values were tested at the beginning, middle, and end of the accepted intervals of each setting. The optimisation that gave the highest classification value out of the three tested start values was considered the most optimised case.

4.3 Frequency study

Another study conducted during this project was a frequency study with the purpose of understanding how the model outputs performance depends on the frequency. This frequency study was based on performance of the models with 6 000 Hz and analysed frequencies below and above 6 000 Hz. The signal was low-pass filtered with different frequencies which created several new signals with varying frequency content. The methodology of *CI 2* and *CI 5* was then conducted for the signals. Output values for the models were produced and an $F_1 - score$ was calculated. This provided insight into what sensor frequency would be needed in an engine to be able to detect cavitation.

In this frequency study, three different tests were performed. The first used the same threshold and trigger settings as for the optimised versions of *CI*. In the second test, no threshold levels were used and in the third experiment, threshold and trigger levels were used to try to maximize the results of the lowest signals that had an F_1 value greater than zero. This was achieved through iterative testing and refinement of threshold and trigger levels. The reason why no full optimisation was done in the third experiment was because there were many signals to optimise. Further, the trigger and threshold levels were very sensitive compared to the amplitude of the signals with lower frequencies. In other words, a full optimisation would only lead to a marginal difference or model outputs will be zero. The reason for adjusting the integral threshold and trigger level across different tests was that these parameters were optimised based on the signal with a maximum frequency content of 6 000 Hz. Consequently, the optimisation was guided by the amplitude characteristics present in those specific signals, which do not necessarily correspond to the amplitudes found within the other analysed signals.

4.4 Correlation analysis

One of the objectives of this thesis is to examine the correlation between the coolant pressure at the liners and the coolant pressure measured by the system sensor. While multiple approaches are possible, the objective of this method is to assess the extent to which the signal from the system sensor can explain the information contained in the signal from the sensors at the liners. Given that the modelling in this project uses the and intersection integral of the local pressure to estimate cavitation, the aim of this methodology is to investigate how the cavitation integral based on the liner pressure correlates to an integral of the measured system pressure. Before outlining the details of the methodological procedure, the delimitations regarding the methodology will be introduced. Since the research question regarding the correlation between the sensors is very broad, the methodological delimitations provide a clearer structural framework and enhances the interpretability of the results from this analysis.

As previously outlined, the purpose of this method is to evaluate how effectively the negative integral, defined as the extent to which the pressure signal from the system sensor falls below the baseline pressure during a specified crank angle interval around TDC, can account for the cavitation integral observed from the sensors mounted at the liners. In order to get a clearer structure for the methodology and get a clearer interpretation of the research question, the following delimitations and assumptions will be made:

1. The Keller PAA-M5-HB absolute pressure sensor is the sensor installed in the experiments and is used in this study to mimic the system pressure sensor. The Keller sensor has a cut off frequency of 50 kHz. Therefore, the analysis will be done based on frequency content up to 50 kHz, which then will be gradually reduced. The justification for this limitation is several. First, the sensor is significantly attenuated at frequencies above 50 kHz. Further, the only high-frequency content of interest is bubble collapse, which only can be detected if the sensor is placed in the vicinity of it (3). Lastly, the frequency study done in chapter 5.3 reveals that a study-based pressure fluctuations in the coolant pressure caused by piston slap can be done by only having up to 3 000 Hz of frequency content in the signal.
2. The analysis will be based on an average value over a specific crank angle interval around TDC where the system pressure sensor will be analysed and against the cavitation integral. The reasons for this are several. First, it is based on the hypothesis that the oscillations used in the modelling of the cavitation integrals can be observed by the system pressure sensor, although in a damped and time-shifted form due to the

distance. Therefore, a crank angle interval near TDC is used to include the correct peaks in the correlation analysis. Further, the analysis is based on the pressure in the entire crank angle interval of interest, which means no sample-by-sample analysis is made. This implies that delays in signal response due to time delay may be considered neglectable. Further the analysis will be done for every engine cycle for each file, which means that the results of each analysed driving case will be integrals that are an average value over several engine cycles.

3. The analysis will be done separately for each proximity sensor position as the damping is expected to be different at different positions. The analysis is therefore divided into three cases: Thrust side cylinder 5, anti-thrust side cylinder 5, and thrust side cylinder 6.
4. Only cavitating cases and cases that fall within a statistical margin of error where the classification is uncertain will be analysed. This is because these cases can be expected to have significant fluctuations in pressure within the crank angle interval of interest. Therefore, these cases would be a good base for an evaluation of a connection between the liner pressure and the system pressure during cavitation, which would provide insight of how good a diagnostic analysis of cavitation could be when using the system pressure sensor.
5. Sensor errors are presumed to be normally distributed.
6. The uncertainty of the cavitation classification is solely based on the combined uncertainty of the sensors, which is given as a combination of linearity error, hysteresis and repeatability. The errors of the individual sensors at the different positions are obtained from the calibration protocols. Several reasons lie behind this limitation. First, the errors given by the manufacturers are referred to as the "worst-case" errors for the sensors. These values are considered the maximum value for an approved sensor, but in most cases the error is much lower than this limit, which is confirmed by the sensors' calibration protocols. Further, the reason why the worst-case values are not used is related to the pressure ranges of the sensors. The Kistler sensor has a pressure range between 0 and 200 bar and the Keller sensor has a pressure range between 0 and 10 bar. The error values are given as a percentage of full-scale pressure, which is valid throughout the whole pressure range. This means that if the "worst-case" values had been used, all negative points would be considered uncertain, which makes this analysis useless.

7. The purpose of selecting these cases is to ensure that instances approaching cavitation is considered in the analysis for correlation, rather to guarantee the inclusion of all cavitating cases. A 100% inclusion of the cavitating points would also incorporate many true negative cases, which would distort the correlation analysis where a foundation is that that cavitation is present.
8. A confidence level of 95% is considered when evaluating the margin of error. The reason why a higher confidence level is not used is because of the purpose described in 7.
9. The temperature uncertainty of the sensors is not considered, as the manufacturers worst-case temperature dependency would expand the error margin significantly and include many true negative cases. As outlined in point 7, the focus is capturing cases close to cavitation rather than ensuring 100% inclusion of the true cases.

4.4.1 Determining cavitating cases

To determine which cases are cavitating or fall within a margin of uncertainty, the following statistical methodology will be used.

According to the delimitations, the uncertainties for the respective sensors specified in the calibration certificates are used with the aim of obtaining the uncertain cases of the cavitation classification. In the calibration certificates, the uncertainty is stated as expanded uncertainty with a confidence level of 95%. (Personal communication with Roger Andersson at Scania, 2025-09-09) This means that the true value is expected to lie within the stated range 95% of the time. The expanded uncertainty is calculated by multiplying the standard uncertainty by a coverage factor, which in this case is 2. A coverage factor of 2 is commonly used because, under the assumption of normal distribution, it corresponds approximately to a 95% confidence interval. This implies that the error for the proximity sensors and the remote sensor can be combined using the methodological procedure presented below where the aim is to find a total error in the system and a new cavitation threshold level that accounts for the uncertainty.

$$U = ku \tag{18}$$

Equation 18 illustrates the expanded uncertainty stated in the calibration certificates where U is the expanded uncertainty stated as a percentage of the full scale pressure for each sensor, which is the highest pressure level in the pressure range of the respective sensor, k is the coverage factor of 2 and u is the standard uncertainty with corresponding coverage factor of 1. To combine the errors from the respective near sensor and the Keller sensor, the combined error U from the respective sensors is summarized using a root square sum illustrated in Equation 19. Since the expanded uncertainties associated with both sensors are based on a coverage factor of 2, it follows that the resulting combined uncertainty is represented with the same coverage factor and confidence level.

$$U_T = \sqrt{{U_1}^2 + {U_2}^2} \tag{19}$$

Equation 19 illustrates the root square sum where U_T is the total standard uncertainty for the sensors, U_1 and U_2 are the uncertainties for the remote sensor and the respective proximity sensor. By choosing a confidence interval of 95%, the expanded uncertainty for the total error can be calculated directly by Equation 19 as the errors for the sensors are given with the same confidence level.

This implies that the cavitation threshold with 95% confidence lies within this margin of error and that cases outside this area would most likely not give a positive outcome when evaluating the classification of cavitation. Furthermore, U_T is used to add an uncertainty factor to the saturation vapour pressure, which means that the cases that could cavitate fulfils the criterion below.

$$x \le P_{sat} + U_T \tag{20}$$

Equation 20 demonstrates the points that will be the base of the correlation analysis between the remote system sensor and the proximity sensors. Where x demonstrates the points that could cavitate based on the presented methodology. This threshold is used for each proximity sensor at the respective positions to extract the points that are cavitating, which are the object of the analysis of correlation between the near sensor and the remote sensor.

Table 4 gives the errors for each sensor, which are used to determine the cases used for the correlation analysis.

Table 4: Overview of the sensors along with their respective measurement uncertainties, reported as expanded uncertainties with confidence level 2 relative to the full-scale pressure of each sensor.

Sensor position	**Model name**	**Error**
Remote sensor	Keller PAA-M5-HB	0.015%
Anti-thrust side cylinder 5	Kistler 603b	0.084 %
Thrust side cylinder 5	Kistler 603b	0.096 %
Thrust side cylinder 6	Kistler 603b	0.153 %

4.4.2 Methodology of correlation analysis

As research question 2, "with what accuracy can the modelled pressure at the cylinder liner correlate to the measured system pressure when cavitation occurs", is broad in scope, the delimitations serve to clearly define the methodological framework. Below follows detailed methodology for how this analysis is carried out and a brief description of how the results from this study can be interpreted.

1. The dataset is divided into three subsets based on the origin of the datafiles, corresponding to each specific liner-mounted pressure sensor, namely the sensors located at the positions thrust side cylinder 5, anti- thrust side cylinder 5 and thrust side cylinder 6. Each of the liner sensors is individually compared to the system pressure sensor, resulting in three distinct cases. This structure enables a position specific evaluation as there may be a strong distance dependency of the dampening of the signals between the sensors.
2. The points then undergo a classification of cavitation based on the methodology presented in section 4.4.1, where the cavitating points according to the new threshold for cavitation are used to calculate the correlation while the remaining points are rejected for this analysis.
3. The signals from the sensors are low-pass filtered based on several frequency limits.
4. The cavitation integral model is applied to the proximity sensor signal based on the new cavitation threshold calculated from the methodology in section 4.4.1. Further, the negative integral, i.e. the integral under the baseline pressure, is calculated from the remote sensor signal. This analysis is done for each engine cycle in the datafiles.
5. A mean value of the absolute value of the integral is calculated over all analysed engine cycles.
6. The root mean square values are analysed with linear regression for all the analysed driving cases according to the line of best fit $I_{Remote} = a\, I_{Proximity} + b$. An R^2 value is calculated and considered to represent the correlation between the remote sensor and the proximity sensors in this application.

The following methodology is used and based on low-pass filters with different frequencies, which means that the result will be three R^2 - values for each frequency. The frequency limits used for the low-pass filtering will be 50 000 Hz, 30 000 Hz, 15 000 Hz, 9 000 Hz, 6 000 Hz, 3 000 Hz, 1 500 Hz, 900 Hz and 300 Hz. Lastly, the window settings that was used for the crank angle domain around TDC was -9° to 26.4° for the proximity sensors, which was the settings obtained from the optimisation of *CI 2,* and -4° to 40° for the remote sensor. The window for the remote sensor was deliberately extended and shifted to account for the time delay between the signals and to ensure that all relevant fluctuations were captured.

4.5 Simulations using different fractions of glycol in the coolant

Another key aspect investigated in this project was the robustness of the models with respect to variations in glycol concentrations in the coolant. The models developed in this study uses the standard composition of the coolant, this applies to both the experiments conducted to generate the experimental data and to the subsequent modelling. As the *CI 2* and *CI 5* models depend on the glycol concentration when calculating the saturation pressure threshold, an interesting investigation involves reducing the glycol concentration to examine whether the integral value increases accordingly. If this is observed, it would indicate that the model is robust to variations in glycol content of the coolant. Conversely, if the integral value rises dramatically when the content of glycol is lowered, it indicates that the baseline pressure level being too close to the saturation pressure level.

This study adopts a relatively straightforward approach. A data point that exhibits significant cavitation, as identified by the *CI 2*, *CI 5*, and *ground truth* models, is analysed under varying glycol concentrations ranging from 0 wt.% to 50 wt.%, in increments of 10 wt.%. The corresponding integral values are then plotted against the glycol composition. Ideally, the slope between each concentration step should remain approximately constant. Minor deviations may occur due to inherent variations in the data. The values of the saturation pressure level are calculated using linearly interpolated values from Table 1. However, this is a simplification since the objective of this study is to ensure that the integral does not diverge when lowering the glycol content. A divergence of the integral would indicate that the saturation pressure level at the given glycol concentration is too close to the regions where the signal exhibits positive values relative to the baseline pressure. This causes a disproportional increase between two consecutive glycol concentrations.

5. Results and Discussion

This section of the report presents the main findings of this study and discusses the results in relation to the research questions. The results are presented by topic beginning with section 5.1, which is the performance of the cavitation models. From this section, *CI 2* and *CI 5* were further analysed as these models demonstrated the highest performance in predicting cavitation.

The performance of the cavitation models is followed by section 5.2, which is the optimisation of *CI 2* and *CI 5*. Section 5.3 examines the result of the frequency study of *CI 2* and *CI 5,* which demonstrates the model's performance across different frequency bands. Further, section 5.4 presents the correlation study between the local pressure at the liners and the global pressure measured by the system sensor. Section 5.5 demonstrates the model´s robustness with respect to variations in glycol content in the coolant. Section 5.6 is the verification of the models where the verification set is used with the optimised settings from section 5.2 to find the performance of *CI 2* and *CI 5*. The discussion of these results will lead to conclusions which are presented and examined in this chapter, summarized in bullet-point form in chapter 6 and followed by suggestions for future research in chapter 7.

5.1 Performance of cavitation models

In this section of the report, the results of the cavitation models will be presented. A scatter plot of the models with its corresponding *ground truth* value, an F_1 – score, and an R^2 value will be presented and discussed for each model. In the end of this section, a table will be presented with an overview of the performance of the calculation models. The results presented in this section is evaluated based on the development set. Regardless, the outcomes from this phase of the study inform the selection of the most promising cavitation models, which are object for continued evaluation and robustness studies.

Since the pressures compared in these plots represent two distinct measurements i.e., the liquid pressure of the coolant and the pressure waves of the bubble collapse against the cylinder, they should not be interpreted as identical. In fact, the order of magnitude between the *ground truth* value and the corresponding model value have different orders of magnitude. The figures in this section therefore uses mean value scaled *ground truth* values to improve the graphical presentation of the plots and to support visual comparison between the plots generated from the different models. For the evaluation of the R^2 version used in this project, a mean value scaled analysis was made according to the statistics presented in section 2.5. Each scatterplot illustrates points, which represents the stationary driving cases analysed. For each scatterplot the x-coordinate represents the scaled *ground truth* value, and the y-coordinate represents the model output.

5.1.1 *Mean 1*

Figure 16 represents the scatter plot for *Mean 1*. The performance of the model is illustrated by the statistical parameters F_1, which is 0, and R^2, which is -0.03. The model has no ability to classify cavitation. This observation can be explained by the fact that the mean value of each file is close to zero, as the files are evaluated over the entire crank angle domain, causing positive and negative fluctuations to cancel out each other. For the cases to show a positive value for cavitation, the saturation pressure level must be over the baseline pressure, which does not happen under the physical conditions given in the analysed cases.

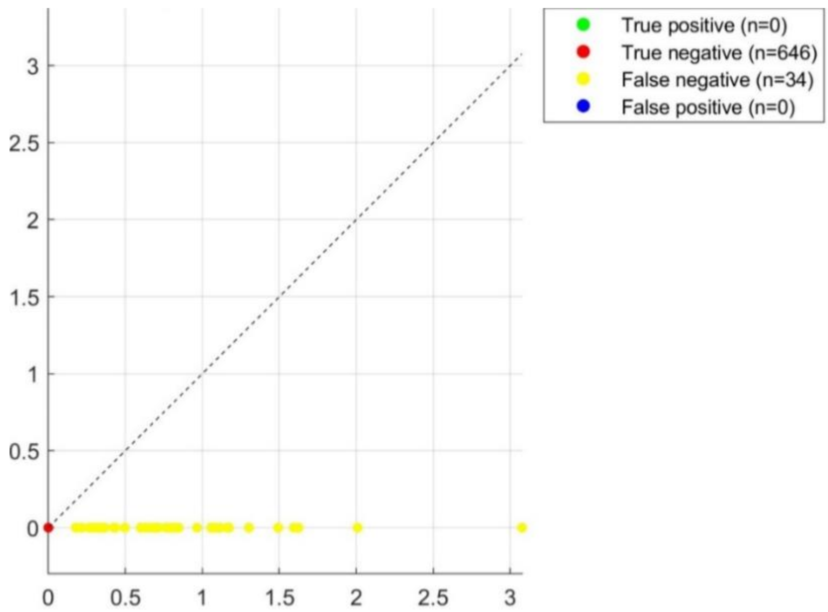

Figure 16: Scatter plot of *Mean 1*-model against scaled *ground truth* values. The y-axis represents the model output (kPa). The x-axis represents the mean value-scaled *ground truth* values (kPa).

5.1.2 *Mean 2*

Figure 17 represents the scatter plot for *Mean 2*. The performance of the model is illustrated by the parameters F_1, which is 0.16, and R^2, which is -4.59. The model has no ability to classify cavitation. This is because of the same reason as for *Mean 1*, with the only difference being that the zero-pressure level is adjusted. It is also possible to observe that the total points of the true positive set and the false negative set combined are equal for *Mean 1* and *Mean 2*. This indicates that there is only a linear difference along the y-axis between Figure 16 and Figure 17, which is due to the offset. A conclusion that could be drawn from the results presented in section 5.1.1 and section 5.1.2 is that a non-linear adjustment is needed to increase the performance of the *Mean* model.

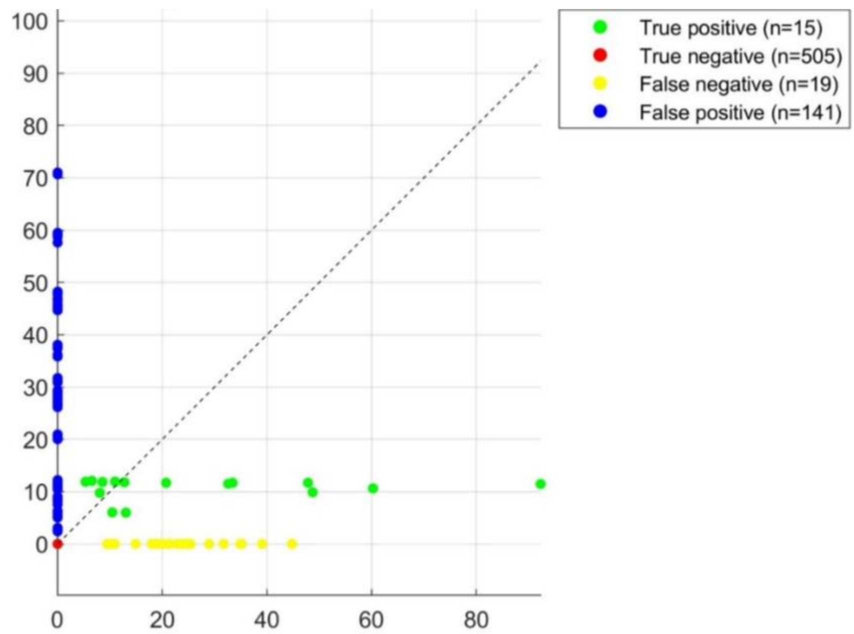

Figure 17: Scatter plot of *Mean 2*-model against scaled *ground truth* values. The y-axis represents the model output (kPa). The x-axis represents the mean value-scaled *ground truth* values (kPa).

5.1.3 *Mean 3*

Figure 18 represents the scatter plot for *Mean 3*. The performance of the model is illustrated by the parameters F_1, which is 0.07, and R^2, which is -0.74. The model has no ability to classify cavitation. Since the model is based on a mean value, the occurrence of false positive points can be attributed to the model's sensitivity to temperature and flow variations. As illustrated in Figure 18, the false positives predominantly correspond to instances of high flow velocities and elevated temperatures, which both contributes to an increased cavitation threshold. On the other hand, the outcome with the false negatives illustrated in Figure 18 align with the reasoning applied for *Mean 1* and *Mean 2,* i.e. that the mean value calculated over the entire crank angle domain remains around the baseline pressure, which in most of the cases lead to a negative outcome when classifying cavitation.

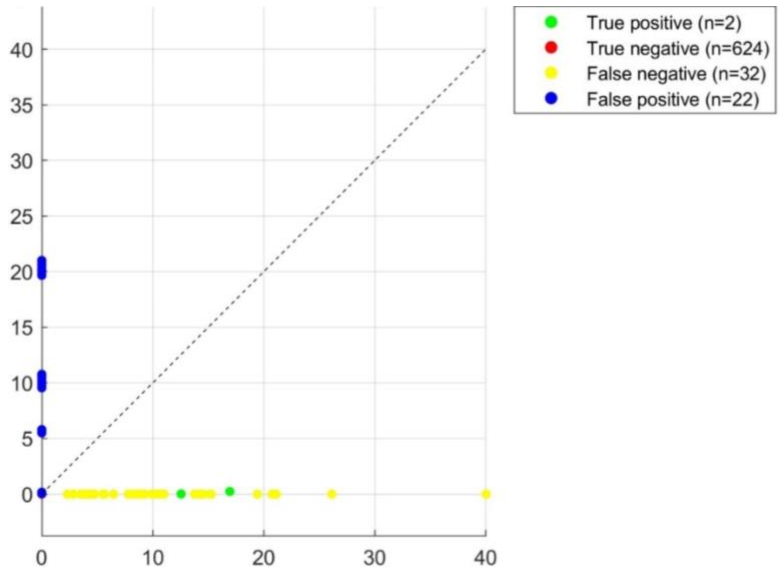

Figure 18: Scatter plot of *Mean 3*-model against scaled *ground truth* values. The y-axis represents the model output (kPa). The x-axis represents the mean value-scaled *ground truth* values (kPa).

5.1.4 Deficit 1

Figure 19 illustrates the scatter plot for *Def 1*. The performance of the model is given by the parameters F_1, which is 0, and R^2, which is -0.03. The model has no ability to classify cavitation. For this model, a sensor with ability to measure higher frequency content is needed because of the condition that only negative values are evaluated. However, as illustrated in Figure 19, the mean value is still above the saturation threshold for cavitation, and no cavitating cases are detected. To further enhance the ability to classify cavitation, an approach that either assess the pressure fluctuations or integrates local temperature and pressure into the modelling framework needs to be developed, given the limitations of the mean value-based methods.

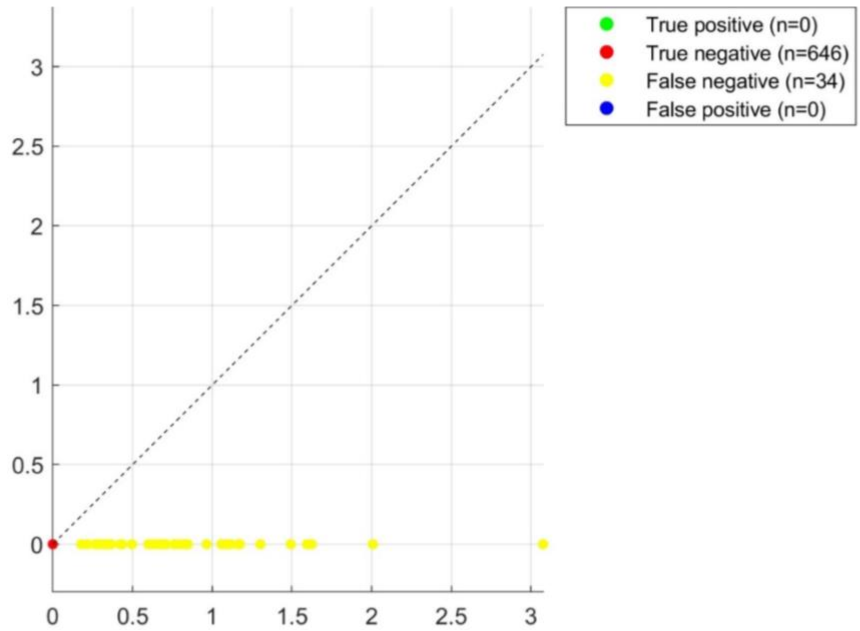

Figure 19: Scatter plot of *Def 1*-model against scaled *ground truth* values. The y-axis represents the model output (kPa). The x-axis represents the mean value-scaled *ground truth* values (kPa).

5.1.5 Deficit 2

Figure 20 represents the scatter plot for *Def 2*. The performance of the model is illustrated by the parameters F_1, which is 0.20, and R^2, which is -2.51. The model has no ability to classify cavitation. The pressure and temperature modelling used for *Def 2* lead to a decrease between the baseline pressure and the cavitation threshold meaning that more points will be false positive. As discussed in section 5.1.4, a modelling approach that evaluates the pressure fluctuations of the coolant is required to ensure that no linear variations in the scatter plots occur between the models, which has been observed results presented thus far.

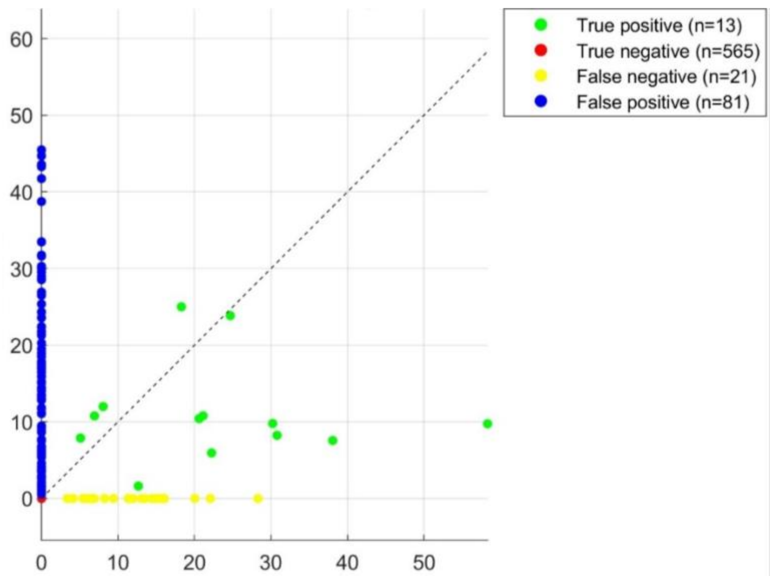

Figure 20: Scatter plot of *Def 2*-model against scaled *ground truth* values. The y-axis represents the model output (kPa). The x-axis represents the mean value-scaled ground truth values (kPa).

5.1.6 *Min*imum 1

Figure 21 represents the scatter plot for *Min 1*. The performance is represented by the statistical parameters F_1, which is 0.36, and R^2, which is -1.99. The model has a no significant ability to classify cavitation. The fact that only one sample in the signal is compared to the cavitation threshold makes this method very sensitive to measurement errors and signal noise. Nevertheless, this also implies that the model, to some extent, functions by comparing the negative fluctuation of the signal to the cavitation threshold. Despite this, the algorithm behind *Min 1* needs further development to be able to classify cavitation correctly.

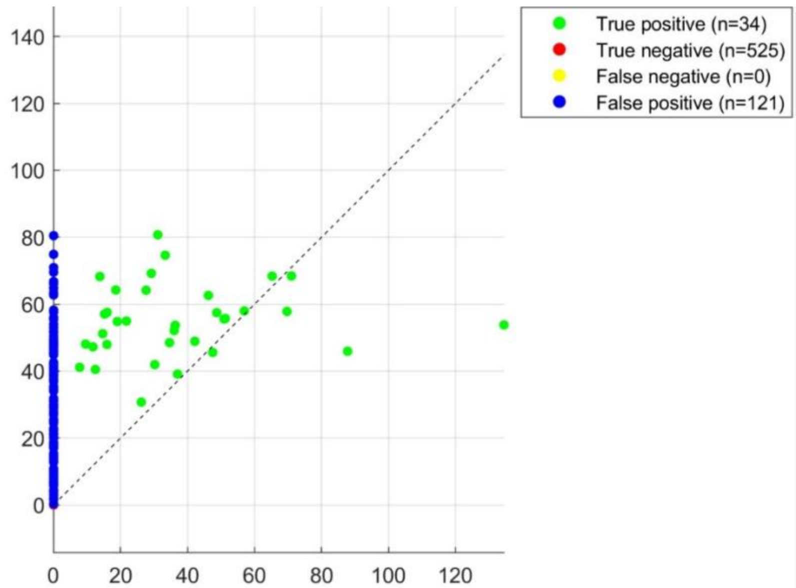

Figure 21: Scatter plot of *Min 1*-model against scaled *ground truth* values. The y-axis represents the model output (kPa). The x-axis represents the mean value-scaled *ground truth* values (kPa).

5.1.7 Minimum 2

Figure 22 illustrates the scatter plot for *Min 2*. The performance of the model is illustrated by the statistical parameters F_1, which is 0.11, and R^2, which is -13.31. The model has no ability to classify cavitation. *Min 2* uses local modelling of the temperature and the baseline pressure level. This, in combination with the minimum of the pressure being used, results in an overshoot of cavitating points. Combining these two modelling approaches results in an overflow of the number of cavitating cases, as the saturation pressure increases while the baseline pressure decreases.

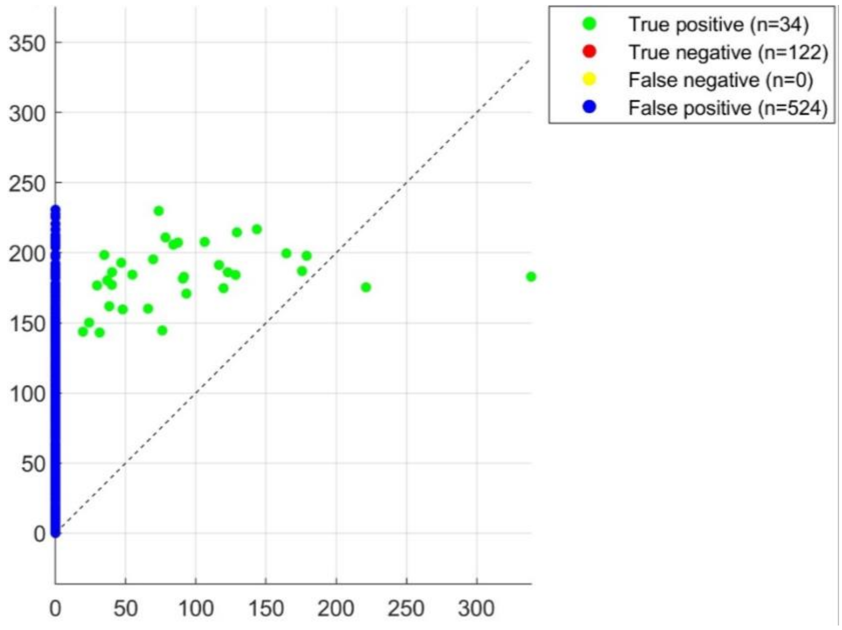

Figure 22: Scatter plot of *Min 2*-model against scaled *ground truth* values. The y-axis represents the model output (kPa). The x-axis represents the mean value-scaled *ground truth* values (kPa).

5.1.8 *CI 1*

Figure 23 illustrates the scatter plot for *CI 1*. The performance of the model is illustrated by F_1, which is 0.22, and R^2, which is -8.41. The model does not have a significant ability to classify cavitation. For *CI 1*, the baseline for the pressure signal is adjusted against the pressure level in the expansion tanks. This results in two main consequences. First, it eliminates the variation of pressure with respect to the pump velocity and engine speed. This does not accurately reflect the system. The expansion tank is unaffected by the pump. In contrast, the pressure signals used in this study are obtained from sensors located after the coolant pump, which makes them influenced by the pump. The second consequence is also linked to the system's design. Since the sensors are positioned downstream of the coolant pump, they register the pressure increase caused by the pump, whereas the expansion tank remains unaffected. A consequence of this is that the baseline pressure for *CI 1* will be too low resulting in more cavitating cases. Therefore, using the expansion tank pressure to model the baseline pressure level will not be good enough to detect cavitation accurately.

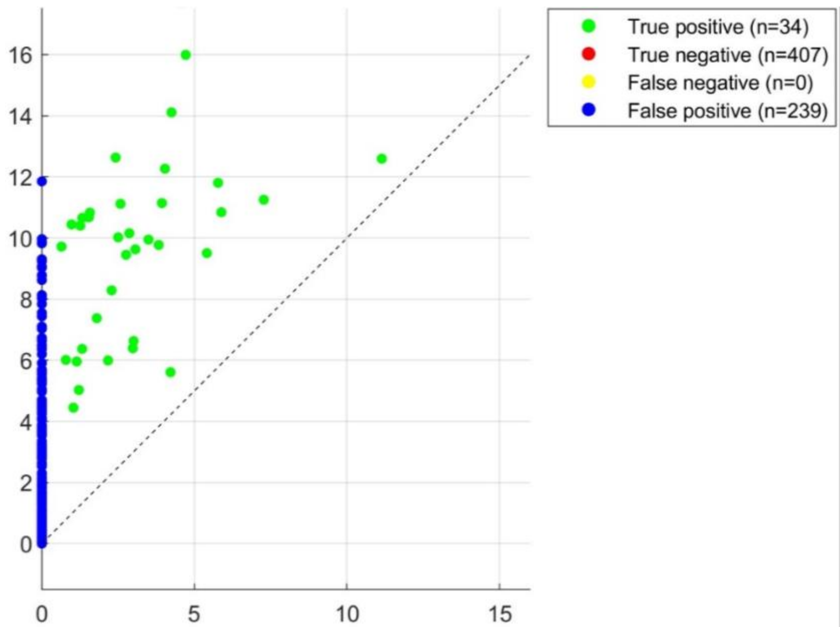

Figure 23: Scatter plot of *CI 1*-model against scaled *ground truth* values. The y-axis represents the model output (kPa). The x-axis represents the mean value-scaled *ground truth* values (kPa).

5.1.9 *CI 2*

Figure 24 illustrates the scatter plot for *CI 2*. The performance of the model is represented by F_1, which is 0.57, and R^2, which is -1.43. The model has an ability to classify cavitation although there are still false positive and false negative cases present. The difference between the modelling approach of *CI 2* compared to for *CI 1* is that the absolute pressure in the block is used as the baseline pressure level for the relative pressure signals. This is a more accurate representation of the system, since variations of the pressure level with respect to engine speed will be incorporated into the model. When using the development dataset, *CI 2* was the model that best classified cavitation and will be evaluated in an optimisation to find the best settings compared to the *ground truth* model. It is important to note that a significant number of false positives can be observed. Upon analysing the parameters for the false positive cases, it becomes evident that many of these cases involve coolant temperatures at 115 $°C$. This results in an increase of the saturation pressure and may indicate boiling of the coolant rather than cavitation. In summary, *CI 2* performs well when classifying cavitation. However, the model is sensitive to changes in the temperature, since the cavitation threshold directly depends upon the temperature.

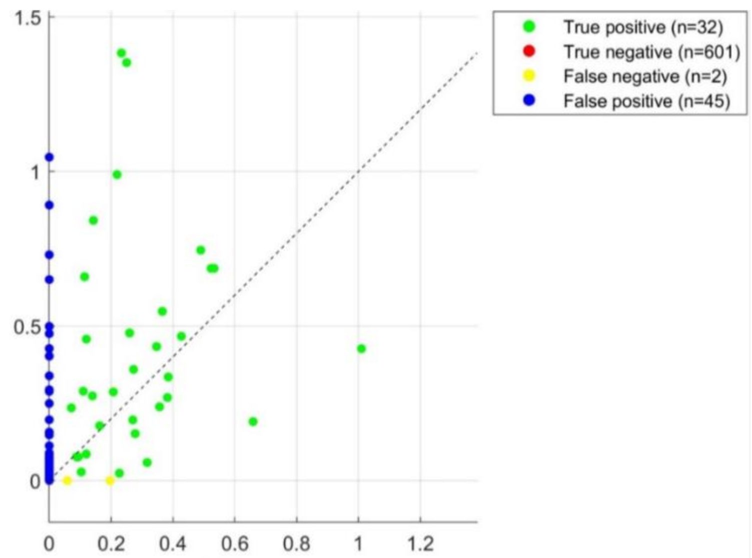

Figure 24: Scatter plot of *CI 2*-model against scaled *ground truth* values. The y-axis represents the model output (kPa). The x-axis represents the mean value-scaled *ground truth* values (kPa).

5.1.10 *CI 3*

Figure 25 illustrates the scatter plot for *CI 3*. The performance of the model is represented by F_1, which is 0.16, and R^2, which is -12.73. The model has a no ability to classify cavitation. The local pressure modelling used in *CI 3* results in a decrease of the baseline pressure level and an overshoot in the number of cavitating cases.

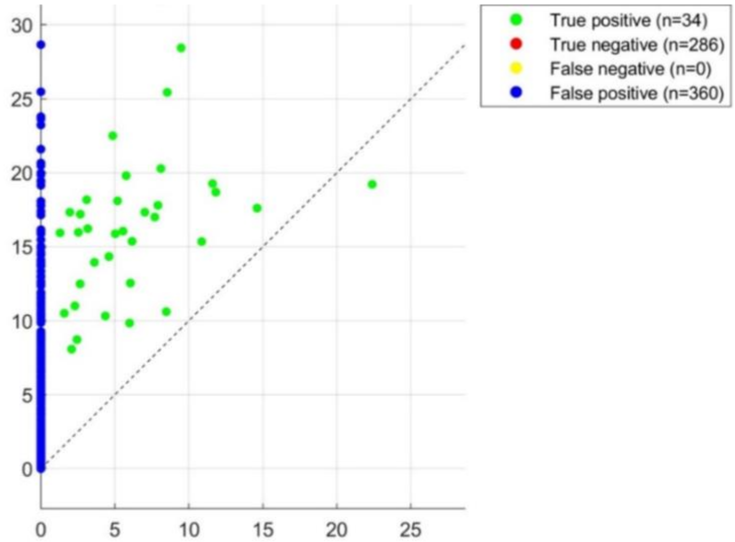

Figure 25: Scatter plot of *CI 3*-model against scaled *ground truth* values. The y-axis represents the model output (kPa). The x-axis represents the mean value-scaled *ground truth* values (kPa).

5.1.11 *CI 4*

Figure 26 illustrates the scatter plot for *CI 4*. The performance of the model represented by F_1, which is 0.15, and R^2, which is -13.10. The model has no ability to classify. The discussion about *CI 4* follows the same reasoning as for *CI 3*. In addition, the local temperature modelling, which uses the end temperature of a hot cylinder contributes to an additional overshoot of cavitating points. This effect is observed when comparing to the results of *CI 3*. To improve the performance of these models, integral threshold levels and trigger levels can be introduced to adjust the evaluation level, thereby making it more difficult for cases to be classified as cavitation.

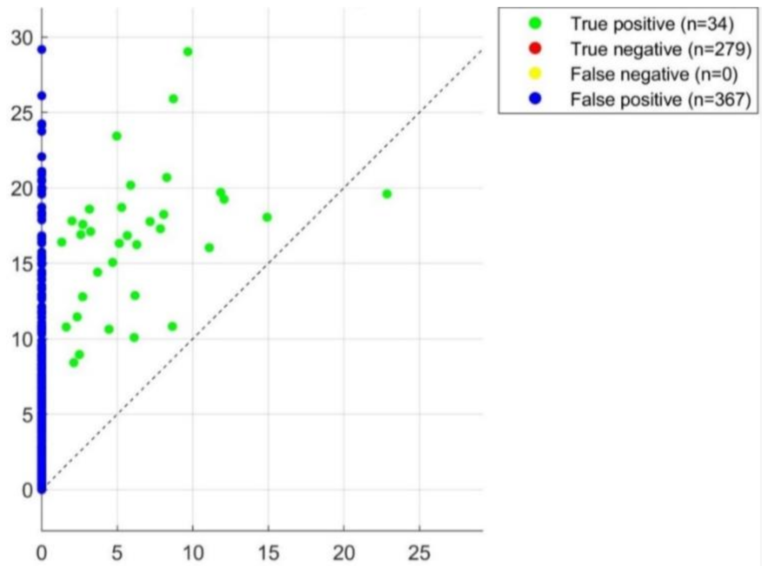

Figure 26: Scatter plot of *CI 4*-model against scaled *ground truth* values. The y-axis represents the model output (kPa). The x-axis represents the mean value-scaled *ground truth* values (kPa).

5.1.12 *CI 5*

Figure 27 represents the scatter plot for *CI 5*. The performance of the model is represented by F_1, which is 0.54, and R^2, which is 0.21. The model has an ability to classify cavitation. However, there are still true positives and true negatives, which makes this model together with *CI 2* objects for optimisation. When introducing an integral threshold and a trigger level, the model's accuracy improved when comparing to *CI 4*. The trigger and the integral threshold were established at a level where noise would be effectively suppressed. Consequently, it is reasonable to assume that pressure fluctuations of a magnitude comparable to overhearing from other cylinders, ambient noise and other disturbances would not classify as cavitation. This model performed second best after *CI 2* in terms of classifying cavitation and best in terms of predicting the level of cavitation. It will therefore be object for an optimisation and a frequency study.

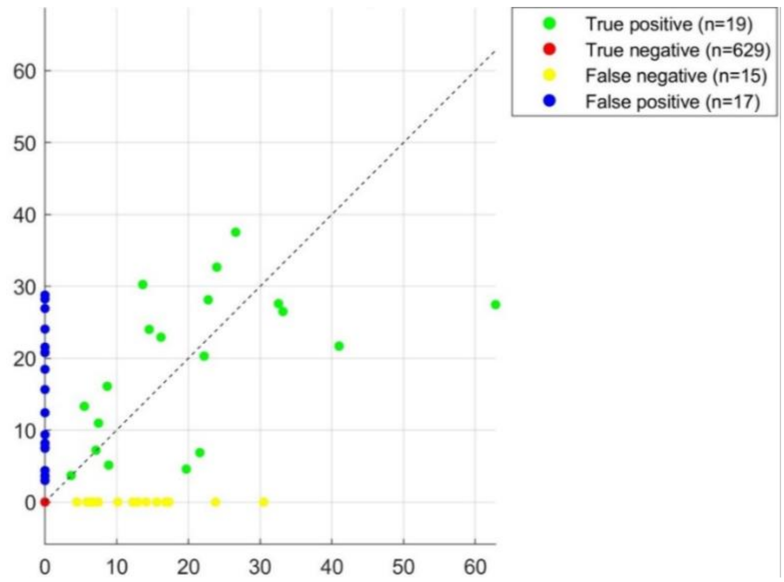

Figure 27 Scatter plot of *CI 5*-model against scaled *ground truth* values. The y-axis represents the model output (kPa). The x-axis represents the mean value-scaled *ground truth* values (kPa).

As illustrated in Figure 27, false positive and false negative values are present along the axes. This reflects different implications for the customer if this model would be used in production engines. The false negative values implies that cases of cavitation would not be detected, which could lead to damage on the cylinder liners that would require expensive repair costs. On the other hand, the false positive points would lead to false alarms, which could lead to consequences as unnecessary time required from the customers and workshop technicians. The underlying reason for the occurrence of false positives and false negatives is found in the strong temperature dependence of the models. By using Equation 5, Antoine's Equation, the models become sensitive to changes in temperature. This can be observed when reviewing the false positive and false negative cases; the false positive have an overrepresentation of points with high temperature and the opposite applies to the false negative cases.

5.1.13 Summary of results for calculation models

Table 5 summarizes the results from the developed cavitation models. The models marked as red showed no potential in predicting cavitation while the models marked as yellow showed potential in predicting cavitation although the result contained misclassifications.

Table 5: Summary of results from developed calculation models.

Model ID	F_1	R^2
Mean 1	0	-0.03
Mean 2	0.16	-4.59
Mean 3	0.07	-0.74
Def 1	0	-0.03
Def 2	0.20	-2.51
5, Min 1	0.36	-1.99
Min 2	0.11	-13.31
CI 1	0.22	-8.41
CI 2	0.58	-1.43
CI 3	0.16	-12,73
CI 4	0.16	-13.10
CI 5	0.54	0.21

As observed in Table 5, the models that performed the best was *CI 2* and *CI 5*. The models could not predict cavitation completely as there still are both false positives and false negatives present for both cases. A deduction from this result is that a diagnostic output using this approach would lead to reduced reliability for the customers. One corrective measure to address false positives and false negatives involves optimizing the models based on maximizing the F_1-score, which will maximize the model's ability to detect cavitation. In addition, another measure to address the problem with false alarms will be to optimise the settings based on false positives. This can be done by a weighting the of false positives compared to false negatives and minimize the total amount of weight. The result of such a study would offer insights into the model's ability to eliminate false alarms.

Another conclusion is that when comparing the models to the benchmark model *Mean 1*, there are several developments that can be made by modelling the baseline pressure and saturation pressure to enable the model to predict cavitation. First, an increase of frequency is needed which captures the fluctuations of the pressure at the liners. From this, several measures are available to either adjust the baseline pressure level or to modify the saturation pressure. However, when both parameters are modelled in a way that decreases the distance between the baseline pressure and the saturation pressure, the model's ability to predict cavitation decreased. As an example, this can be observed from *CI 3* and *CI 4* as the output from these models results in an overshoot in the number of cavitating cases. Therefore, using the thresholds described in the methodology for *CI 5* is a reasonable measure to avoid overshoot of cavitation points due to the model's sensitivity to pressure, temperature, and flow rate. A conclusion is that two measures that both decreases the distance between the saturation threshold and the baseline pressure level is not representing the reality.

5.2 Cavitation Integral with optimised settings

The optimisation in this section is done with respect to F_1 and F_β, and the result of the optimisation is presented below. The results presented are based on the development set and the main findings of the optimisation are the settings, which will be used for further analyses in this study.

Table 6: Optimised settings and results for *CI 5*

Optimisation nr.	Threshold	Trigger	Window start	Window end	F_1	R^2
1.	25 kPa	40 kPa	-4°	36.4°	0.62	0.31
2.	18.5 kPa	0 kPa	-32°	36.9°	0.43	0.22

Table 6 presents the optimised settings of *CI 5.* The optimisation with the aim of maximizing F_1 reached a performance of 0.62 and the optimisation of F_β reached a performance of 0.43.

Optimisations number 1 is an optimisation with the aim of maximizing F_1. Optimisations 2 is an optimisation to maximize F_β. As illustrated in Table 7, the two optimisations resulted in different settings, which illustrates that the two optimisations were successful.

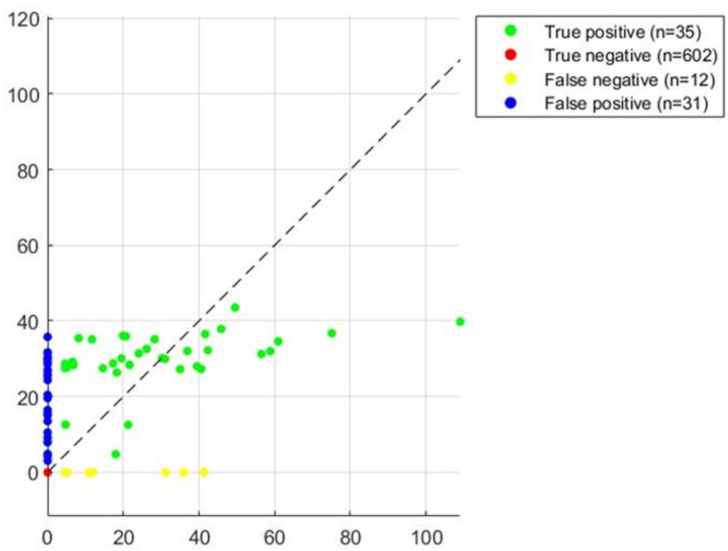

Figure 28: Scatter plot of *CI 5* optimised to maximise F_1. The y-axis represents the model output (kPa). The x-axis represents the mean value-scaled *ground truth* values (kPa).

Figure 28 illustrates the scatter plot of the result obtained from the optimisation of settings with the aim to maximize F_1. The figure illustrates the increased performance after optimisation with more true positives compared to the scatter plot in section 5.1.12.

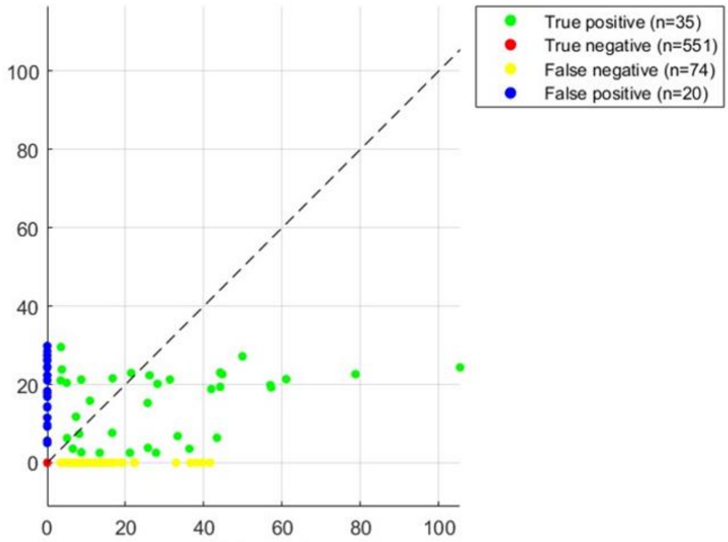

Figure 29: Scatter plot of *CI 5* optimised to maximize F_β. The y-axis represents the model output (kPa). The x-axis represents the mean value-scaled *ground truth* values (kPa).

Figure 29 represents the scatter plot of the results obtained from the optimisation with the aim of maximizing F_β. The figure illustrates that the objective of the optimisation was successful with less false positives. Although the false positive points drop from 31 to 20, the downside of the optimisation is that the false negative points increase from 12 to 74. Seen from a performance perspective, the F_1 score decreases to 0.41. However, the precision increases, with the true positives remaining consistent and the false positives decreasing. Based on the results of the optimisation, the result is deemed insufficient, as the number of false positives remains considerable. A recurring trend observed among the remaining false positives is the overrepresentation of cases with cooling temperature of 115 $°C$ and high pump velocities. This phenomenon may be attributed to the modelling of *CI 5*, which directly incorporates flow velocity. Further, elevated temperatures contributed to a higher saturation threshold making the model highly sensitive to temperature variations.

Table 7: Optimised settings and results for *CI 2*.

Optimisation nr.	Threshold	Trigger	Window start	Window end	F_1	R^2
1.	0 kPa*	0 kPa*	-9°	26.4°	0.71	-0.50
2.	0 kPa	6 kPa	-9°	26.4°	0.74	-0.52
3.	0 kPa	20 kPa	-9°	38.4°	0.48	0.06

*The threshold and trigger was not used in the optimisation

Table 7 presents the results from the optimisation of *CI 2*. Optimisation 1 and 2 optimised the F_1, while optimisation 3 optimised the F_β. The difference between optimisation 1 and 2 was that the threshold and trigger levels used in *CI 5* was introduced.

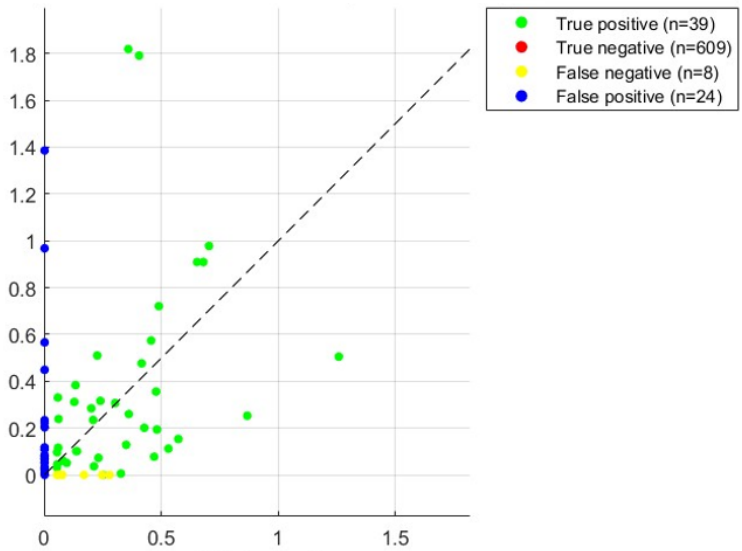

Figure 30: Scatter plot of *CI 2* values with optimised to maximise F_1. The y-axis represents the model output (kPa). The x-axis represents the mean value-scaled *ground truth* values (kPa).

Figure 30 illustrates the result of optimisation 1. The performance is represented by the F_1 of 0.71. The improved performance is illustrated by the increase of true positives and decrease of false positives.

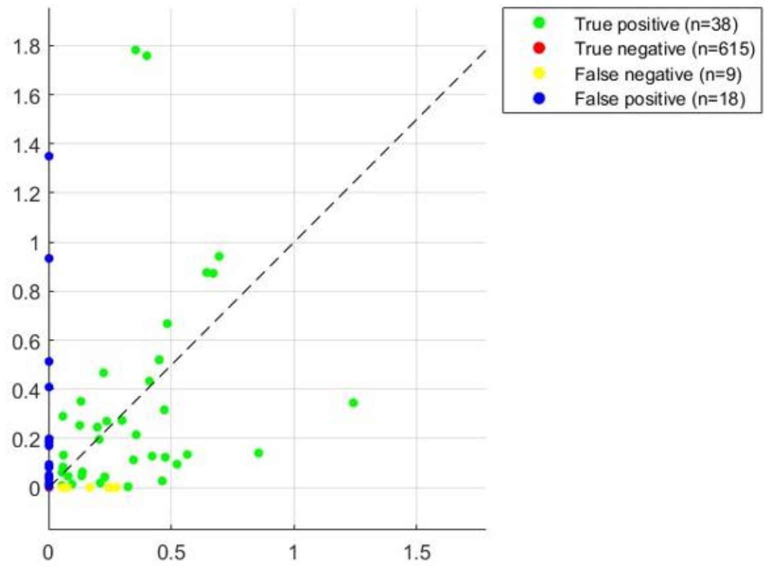

Figure 31: Scatterplot of optimised *CI 2* values when trigger and threshold levels was introduced. The y-axis represents the model output (kPa). The x-axis represents the mean value-scaled *ground truth* values (kPa).

Figure 31 illustrates the scatter plot of the result from optimisation 2. The optimisation performed an F_1 of 0.74 making it the best performing model based on the development set. As mentioned in 4.2, the start values of the thresholds and trigger was set to zero with the intention of testing if the settings would contribute to a better result. This was confirmed by the increase of the trigger level to 6 kPa and 18.5 kPa for optimisation 2 and 3.

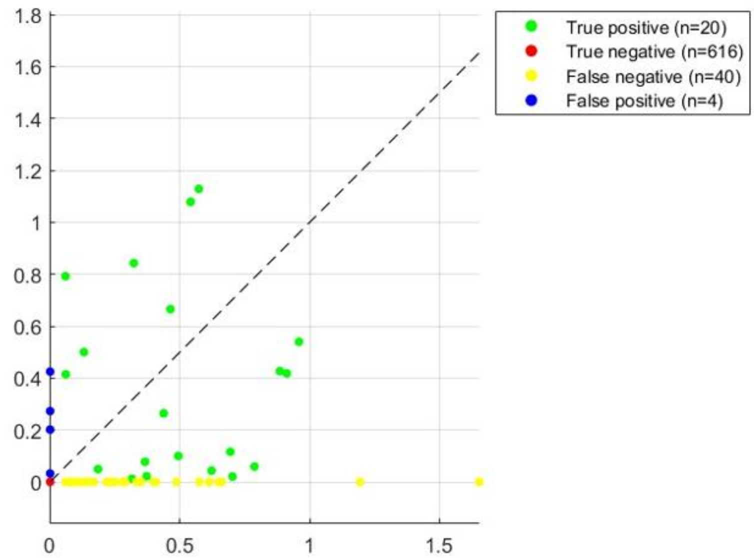

Figure 32: *CI 2* values optimised on the criterion of maximizing F_β. The y-axis represents the model output (kPa). The x-axis represents the mean value-scaled *ground truth* values (kPa).

Figure 32 illustrates scatter plot of the results from optimisation 3. The F_1-score was 0.48. The optimisation was successful with only four false positives. However, based on the overall results of the optimisation, the optimisation is deemed insufficient, as the number of false negatives remains considerable. Further, there were only four FP points, which is a good indication that the optimisation was successful. Additionally, an observation is that all four of true positives were cases with coolant temperature of 115 $°C$, which leads back to the previously discussed issue regarding the model's sensitivity to temperature. A conclusion from this is that the models developed in this study are very sensitive to temperature and that another approach for the temperature modelling is necessary to address the problem with the temperature dependency on the cavitation classification. Moreover, the results indicate a strong ability to classify cases with coolant temperature of 90 $°C$, since the false negatives exhibits a contrasting pattern with coolant temperatures lower than 90 $°C$.

5.3 Frequency study

A frequency study with the aim to investigating how the frequency will change the performance of the models has been conducted with the *CI 2* and *CI 5* models. This section presents and discusses the results from the frequency study.

Table 8: Classification performance of the models at different frequencies with optimised settings.

Frequency limit	F_1 CI **2**	F_1 CI **5**
300	0	0
600	0	0
1 200	0	0.34
2 400	0.68	0.62
6 000	0.74	0.62
12 000	0.70	0.60
25 000	0.70	0.60
102 400	0.70	0.62

Table 9: Classification performance of models at different frequencies without trigger and threshold levels.

Frequency limit	F_1 CI **2**	F_1 CI **5**
300	0	0.19
600	0	0.28
1 200	0	0.27
2 400	0.72	0.21
6 000	0.71	0.19
12 000	0.69	0.19
25 000	0.70	0.19
102 400	0.72	0.18

Table 10: Classification performance of models at different frequencies with modified trigger and threshold levels to maximize the classification of the signals with the lowest frequencies.

Frequency limit	F_1 CI **2**	F_1 CI **5**
300	0	0
600	0	0
1 200	0	0.49
2 400	0.72	0.46
6 000	0.71	0.47
12 000	0.69	0.46
25 000	0.70	0.46
102 400	0.73	0.47

Table 8-10 illustrates the performance of the models *CI 2* and *CI 5* when low pass filters are applied. The models' ability to classify cavitation is almost constant until 2 400 Hz for *CI 2* and 1 200 for *CI 5*. A conclusion drawn from this result is that the raw signal sampled at 204 800 Hz includes frequency content above 2 400 Hz that is important for the modelling of *CI 2* and *CI 5*. Therefore, a sensor would need to be able to measure frequencies up to at least 2 400 Hz for these models to be successful. Furthermore, the ability to classify cavitation above these frequencies remain constant, which can be seen from the fact that the performance is approximately constant for the frequencies over 2 400 Hz.

5.4 Correlation analysis of sensor at liners and system sensor

The following section outlines the result and discussion about the correlation analysis of the system pressure and the coolant pressure at the liners. The tables in this section presents the R^2 value as well as the number of cases included in each calculation, which depend on the saturation pressure threshold and the errors of the sensors.

Table 11: Results of the correlation analysis for a sensor at cylinder 5 ATS and a remote sensor.

Frequency	R^2	Total points
50 000 Hz	0.16	57
30 000 Hz	0.16	56
15 000 Hz	0.14	54
9 000 Hz	0.13	53
6 000 Hz	0.14	51
3 000 Hz	0.07	50
1 500 Hz	0.09	21
900 Hz	0	0
300 Hz	0	0

Table 11 presents the result for the correlation between the remote sensor and the proximity sensor mounted at the anti-thrust side of cylinder 5. The result demonstrates that the correlation between the integral for the remote sensor and the integral for the proximity sensor is weak. The result also reveals that there are many cases close to the cavitation threshold, which is evident from the decreasing number of data points as the frequency decreases.

Another important finding from this study can be observed from the performance of the different frequencies. The lowest frequency at which this analysis can be done is 1 500 Hz. However, a substantial loss of cases is observed between 3 000 Hz and 1 500 Hz. This observation aligns with the findings from the frequency study presented in section 5.3, where it was shown that the performance drops in the ranges between 2 400 Hz and 1 200 Hz as well as 1 200 Hz and 600 Hz. The conclusion that approximately 2 400 Hz to 3 000 Hz is the frequency limit needed for the modelling and analyses in this project therefore remains. However, the results from ATS show that a diagnostic output based on the integral of the remote sensor would not be sufficient to diagnose the amount of cavitation.

Table 12: Results of the correlation analysis for a sensor at cylinder 5 TS and a remote sensor.

Frequency limit	R^2	Total points
50 000 Hz	0.31	32
30 000 Hz	0.30	30
15 000 Hz	0.30	28

9 000 Hz	0.31	27
6 000 Hz	0.32	27
3 000 Hz	0.31	27
1 500 Hz	0.53	15
900 Hz	0	0
300 Hz	0	0

Table 12 illustrates the results for the correlation between the proximity sensor at the position at the thrust side of cylinder 5 and the remote sensor. Fewer points cavitated at this position compared to position 5 ATS. However, at the TS position higher correlation was observed. A similar conclusion could be drawn regarding the proximity of the data points to the cavitation threshold of this analysis. This is supported by the observation that the data points included in the analysis decreases with decreasing frequency. Conversely, the correlation increases with decreasing frequency, which could be a sign that the correlation is stronger at the points that are cavitating significantly. Nevertheless, the correlation is not sufficient to be able to make a diagnosis of the amount of cavitation.

Table 13: Results of the correlation analysis for a sensor at cylinder 6 TS and a remote sensor.

Frequency	R^2	**Total points**
50 000 Hz	0.09	34
30 000 Hz	0.06	34
15 000 Hz	0.05	32
9 000 Hz	0.06	31
6 000 Hz	0.03	31
3 000 Hz	0.14	29
1 500 Hz	0.20	20
900 Hz	0	0
300 Hz	0	0

Table 13 illustrates the results of the correlation analysis between the pressure at the thrust side of cylinder 6 and the remote sensor.

For this position, similarly to the position at the thrust side of cylinder 5, the number of points decreases with frequency. This seems to be a trend for all three cases, which means that the uncertainty analysis that was done before played a role and has been shown to have an impact on the number of points. Furthermore, there is a weak correlation and compared to the sensor at the thrust side of cylinder 5, the correlation here is weaker. This can be explained by the fact that this sensor is located furthest from the remote sensor.

Several observations can be made from this correlation study. First, the number of cavitating cases according to the cavitation integral differs between the thrust and anti-thrust side. Furthermore, a frequency band up to 3 000 Hz is required to conduct an analysis based on the pressure waves caused by the piston slap. This observation can also be confirmed from the results presented in chapter 5.3.

The conclusions from the correlation analysis are also several. First, the results indicate that the correlation between the system pressure sensor and the proximity sensor is weak. This suggest that the methods that evaluates the integral at the system pressure sensor is not sufficient to estimate the amount of cavitation on the cylinder liner. This implies that a diagnostic output using this method would be ineffective. A future study that would complement this corelation analysis would be to investigate the possible to classify cavitation by examining the pressure at the remote sensor. Such a study could utilize a method like *ground truth* that quantifies cavitation using the bubble collapse and thereby provide ground truth of the cavitation, which a classification could be compared against. A correct classification using the system pressure sensor could enable a diagnostic assessment to be performed, either through workshop technicians or trough automated means. As previously mentioned in chapter 5.2, the amount of cavitation cannot be estimated from the pressure fluctuations caused by piston slap. However, a classification could be achieved by implementing an alternative temperature modelling approach. This method could also be examined using data from the system sensor position.

5.5 Simulation of cavitation integral with varied compositions of glycol

This section of the report presents the results of the robustness of the models with respect to the concentration of glycol in the coolant.

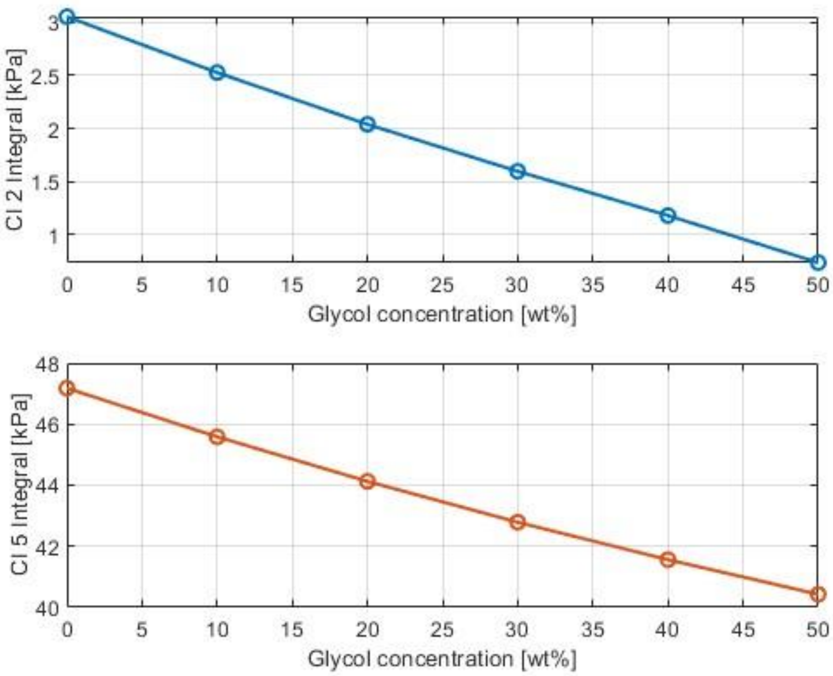

Figure 33: The robustness of the models with respect to glycol concentration.

As illustrated in Figure 33, both models are robust with respect to the glycol concentration. Worth noting, is that the measurements are made with a standard coolant that has 50 vol% glycol. A more precise study would be to vary the coolant composition in experiments to account for other physical parameters of the coolant as well. However, the results of the robustness study indicates that the framework used in the models are robust with respect to different coolant compositions.

5.6 Verification of the result

As findings of this thesis indicate that a diagnostic use of the models could result in unreliable outcomes including false alarms and undetected cavitation events, this section of the report outlines the verification of the result using the verification data set. The verification data set was used for the calculations for the models *CI 2* and *CI 5* with the aim to verify the result from the modelling.

Tabell 14: The verification of the models.

Model ID	F_1	R^2
CI 2	0.46	-2.02
CI 5	0.71	0.25

Table 14 presents the final performance of models. The result is that *CI 5* is the model that both classifies cavitation and predicts the amount of cavitation best.

One observation that should be pointed out is that this result obtained from the independent verification data contradicts what the development data illustrated. The result from the development showed that the model *CI 2* classified cavitation better than the model *CI 5*. The uncertainty between the verification and the development results could be due to several factors. A possible but unlikely reason would be that the model *CI 2* specifically may have been overfitted to patterns specific to the development data. The cause why this reason is unlikely is that the splitting of the data set was done with respect to the subsets that the data was delivered as. This classified the data based on system pressure and coolant temperature, which gave the development set and the verification set a fairly equal distribution between types of data points. Furthermore, the development of the models has not involved extensive development of the same model. The adjustments made have included exploration of alternative modelling approached and fine-tuning of the settings for both *CI 2* and *CI 5,* which reduces the likelihood of an overfitting of *CI 2.* What may underlie the observation, is that the data set has a large imbalance between class distribution. In the development set, there are approximately 60 positive points according to the *ground truth* model and in the verification set there were six points, which indicates an imbalance of positive points. With a larger number of positive cases, the results observed have good prospects of being robust against single misclassifications in the form of false positives and false negative points. On the other hand, a misclassification is made in the validation implies that 16% of the positive points are affected, which makes the validation extremely sensitive. An improvement to a cavitation study would therefore be to obtain a greater proportion of positive points in relation to negative points. Partly so that occasional misclassifications would not affect the verification as much, but also so that the verification of the result would be more reliable.

The models' ability to estimate the amount of cavitation is similar between development and validation. *CI 5* predict the amount of cavitation best. An interesting observation that could form the basis for further research, is the similarities of the results of *CI 5* and the results that can be observed in chapter 5.4 when the frequency decreases. Since *CI 5* uses a trigger level and an integral threshold level, it provides an insurance that only the cases that cavitate significantly will be analysed. This may also be observed when the correlation increases with decreasing frequency while the number of cavitating points decreases. In the latter case, the points that do cavitate significantly will be the points that are present in the signals with lower frequencies. In a future research study, the relationship between the piston slap mechanism and points that cavitate significantly could be analysed to see if a correlation between bubble collapse level and piston slap level exists. This observation is not a conclusion that is confirmed by this study, because the basis for these observations is insufficient to draw a conclusion from; however, it is an observation made that results in a hypothesis that can be tested in a more in-depth and targeted investigation.

In summary, *CI 5* is the model that can best predict cavitation both in a classification context and cavitation level context. However, several adjustments would be necessary to develop a model to be the basis for a cavitation diagnosis. First, a more robust temperature modelling would be needed. Second, a larger dataset would also be needed. This would lead to development of the models with a stronger foundation in temperature dependency and a more reliable verification.

6. Conclusion

This section of the report summarizes the main conclusions of the thesis.

- *CI 5* is the best model for the prediction of cavitation.
- The hypothesis was not confirmed. It stated that the pressure difference between the coolant pressure and the saturation pressure at the liners, at cavitation onset, would be proportional to the cavitation intensity.
- The pressure difference between the coolant pressure and the saturation pressure threshold serves as a reliable indicator for cavitation classification. However, to enhance the robustness of the classification, an alternative approach to model the temperature and flow rate is required.
- Models that incorporate two modelling steps that both reduces the distance between the baseline pressure level and the saturation pressure level tend to give results that deviate from the actual system behaviour.
- A bandwidth up to approximately 3 000 Hz is required in the pressure signals from the liners to be able capture pressure waves caused by the piston slap.
- The correlation analysis reveals a weak relationship between the integral of the system pressure and the cavitation integral, indicating that the level of cavitation cannot be reliably estimated using the system sensor alone. As a result, any diagnostic output based on this pressure sensor for estimating cavitation levels would lack sufficient accuracy.
- The cavitation integral is robust to changes in glycol concentration in the coolant.

In summary, these conclusion highlights the limitations of the current modelling approach using the pressures from the sensors presented in this master thesis. The conclusions also underscore the need for a more robust modelling approach regarding the temperature and flow rate. Finally, the conclusions emphasize that the hypothesis regarding the pressure difference between the coolant pressure and the saturation pressure threshold does not serve as a reliable indicator of the cavitation level. However, as seen in the modelling of this study, these two pressures can be used when the aim is to classify cavitation events.

7. References

1. Zhou YK, Hammitt FG. Cavitation Damage of Diesel Engine Wet-Cylinder Liners. In SAE International; 1990 [cited 2025 Aug 21]. Available from: https://saemobilus-sae-org.focus.lib.kth.se/papers/cavitation-damage-diesel-engine-wet-cylinder-liners-900437

2. Javanmardi D, Rezvani MA. Thermomechanical Fracture Failure Analysis of a Heavy-Duty Diesel Engine Cylinder Liner through Performance Analysis and Finite Element Modeling. SAE Int J Engines. 2020 Oct 2;13(5):665–83.

3. Steck B, Sommerfeld G, Schneider V. Cavitation on Wet Cylinder Liners of Heavy Duty Diesel Engines. In SAE International; 2006 [cited 2025 Aug 21]. Available from: https://saemobilus-sae-org.focus.lib.kth.se/papers/cavitation-wet-cylinder-liners-heavy-duty-diesel-engines-2006-01-3477

4. Zade GA, Gadekar DD. Accelerated Simulation of Engine Wet Cylinder Liner Cavitation Test Procedure. In The Automotive Research Association of India; 2007 [cited 2025 Aug 21]. Available from: https://saemobilus-sae-org.focus.lib.kth.se/papers/accelerated-simulation-engine-wet-cylinder-liner-cavitation-test-procedure-2007-26-023

5. Liu D, Li G, Sun N, Zhu G, Cao H, Wang T, et al. Vibration-induced cavitation in cylinder liners caused by piston slaps. Int J Mech Sci. 2024 Apr 1;267:109025.

6. Glyniadakis GV, DAgostini MFH, Casagrande M. Liner Vibration and Cavitation. In SAE International; 2006 [cited 2025 Aug 21]. Available from: https://saemobilus-sae-org.focus.lib.kth.se/papers/liner-vibration-cavitation-2006-01-2512

7. Demarchi V, Windlin FL. Cavitation Erosion on Cylinder Liners. In SAE International; 1995 [cited 2025 Aug 21]. Available from: https://saemobilus-sae-org.focus.lib.kth.se/papers/cavitation-erosion-cylinder-liners-952250

8. Steck B. Avoiding Cavitation on Wet Cylinder Liners of Heavy Duty Diesel Engines by Parameter Changes. In SAE International; 2008 [cited 2025 Aug 21]. Available from: https://saemobilus-sae-org.focus.lib.kth.se/papers/avoiding-cavitation-wet-cylinder-liners-heavy-duty-diesel-engines-parameter-changes-2008-36-0073

9. Bederaux-Cayne WS. Quantifying Parameters Relevant to Liner Cavitation on a Diesel Engine. In SAE International; 1996 [cited 2025 Aug 21]. Available from: https://saemobilus-sae-org.focus.lib.kth.se/papers/quantifying-parameters-relevant-liner-cavitation-a-diesel-engine-960881

10. Davis GD, Christ RJ. A Comparison of Engine Coolant in an Accelerated Heavy Duty Engine Cavitation Test. In SAE International; 1996 [cited 2025 Aug 21]. Available from: https://saemobilus-sae-org.focus.lib.kth.se/papers/a-comparison-engine-coolant-accelerated-heavy-duty-engine-cavitation-test-960883

11. Liu D, Li G, Sun N, Zhu G, Li L, Wang T, et al. Modelling and analysis of the vibro-acoustic coupling behaviours of the cylinder liner-water jacket system towards cavitation prediction. Mech Syst Signal Process. 2025 Feb 15;225:112307.

12. Hong F, Tian H, Yuan X, Liu S, Peng Q, Shi Y, et al. CFD-assisted modeling of the hydrodynamic cavitation reactors for wastewater treatment — A review. J Environ Manage. 2022 Nov 1;321:115982.

13. Green GW, Engelstad RL. A Technique for the Analysis of Cylinder Liner Vibrations and Cavitation. In SAE International; 1993 [cited 2025 Aug 21]. Available from: https://saemobilus-sae-org.focus.lib.kth.se/papers/a-technique-analysis-cylinder-liner-vibrations-cavitation-930582

14. Shen J(沈钧炜), Tang X(汤小凤), Liu W(刘闻达), Ma S(马少武), Luo P(罗鹏), Zhang Y(张宇宁), et al. Bubble dynamics near a flat wall and a cylinder within confined spaces. Phys Fluids. 2025 Jan 3;37(1):013307.

15. Shen J(沈钧炜), Zhang S(张书瑞), Tang X(汤小凤), Xu Q(徐启航), Zhang T(张婷婷), Liu W(刘闻达), et al. Dynamics of a laser-induced bubble near a cylinder within a confined space. Phys Fluids. 2024 Oct 16;36(10):103353.

16. Zhang X(张湘晴), Yang C(杨辰昕), Wang C(王聪涛), Zhang Y(张宇宁), Zhang Y(张宇宁). Dynamics of an oscillating cavitation bubble within a narrow gap. Phys Fluids. 2023 Oct 3;35(10):103302.

17. Nguyen QT, Nguyen VT, Phan TH, Duy TN, Park SH(박성호), Park WG(박원규). Numerical study of dynamics of cavitation bubble collapse near oscillating walls. Phys Fluids. 2023 Jan 5;35(1):013306.

18. Gummer JH, Thew MT. Venturi investigations into cavitation in ethylene glycol/water mixtures. Proc Inst Mech Eng Part E J Process Mech Eng. 1998 Nov 1;212(4):235–50.

19. BASF. GlytherminNF-TDS.pdf [cited 2025 Sept 1]. Available from: https://www.deserkimya.com/public/uploads/images/Kataloglar/GlytherminNF-TDS.pdf

20. Scribd.com. [cited 2025 Aug 30]. Cooling Scania | PDF | Thermostat | Radiator. Available from: https://www.scribd.com/document/494880657/cooling-scania

21. Turney S. Coefficient of Determination (R^2) | Calculation & Interpretation [Internet]. Scribbr. 2022 [cited 2025 Aug 21]. Available from: https://www.scribbr.com/statistics/coefficient-of-determination/

22. MathWorks. Coefficient of Determination (R-Squared) - MATLAB & Simulink [Internet]. [cited 2025 Aug 21]. Available from: https://se.mathworks.com/help/stats/coefficient-of-determination-r-squared.html

23. Laiba Siddiqui. Coefficient of Determination: What R-Squared Tells Us [Internet]. [cited 2025 Aug 21]. Available from: https://www.datacamp.com/tutorial/coefficient-of-determination

24. Rohit Kundu. F1 Score in Machine Learning: Intro & Calculation [Internet]. [cited 2025 Aug 21]. Available from: https://www.v7labs.com/blog/f1-score-guide

25. Hicks SA, Strümke I, Thambawita V, Hammou M, Riegler MA, Halvorsen P, et al. On evaluation metrics for medical applications of artificial intelligence. Sci Rep. 2022 Apr 8;12(1):5979.

26. Sokolova M, Japkowicz N, Szpakowicz S. Beyond Accuracy, F-Score and ROC: A Family of Discriminant Measures for Performance Evaluation. In: AI 2006: Advances in Artificial Intelligence [Internet]. Springer, Berlin, Heidelberg; 2006 [cited 2025 Aug 22]. p. 1015–21. Available from: https://link.springer.com/chapter/10.1007/11941439_114

27. Ernst Schmidt KW. Wärmeübergang bei der Umströmung von Zylindern,[In German]. Cited in Thermopedia, Cross Flow Heat Transfer (https://www.thermopedia.com/content/675/). Forsch Auf Dem Geb Ingenieurwesens. 1941;12:65–73.

28. Werner Lohrisch. Forschungsarbeiten auf dem Gebiete des Ingenieurwesens, Vol. 322, s. 46 [In German]. Cited in Thermopedia, Cross Flow Heat Transfer (https://www.thermopedia.com/content/675/). Forsch Auf Dem Geb Ingenieurwesens. 1929;322:46.

29. J.M. Coulson JFR. Chemical Enginnering. 4th edn. Oxford: Pergamon Press; 1990. 708 p. (Chemical Engineering; vol. 1).

30. Churchill SW, Bernstein M. A Correlating Equation for Forced Convection From Gases and Liquids to a Circular Cylinder in Crossflow. J Heat Transf. 1977 May 1;99(2):300–6.

31. Houghton EL, Carpenter PW, Collicott SH, Valentine DT. Equations of Motion. In: Aerodynamics for Engineering Students [Internet]. Elsevier; 2017 [cited 2025 Aug 22]. p. 87–149. Available from: https://linkinghub.elsevier.com/retrieve/pii/B978008100194300002X

32. T. Baracu RB. ResearchGate. [cited 2025 Aug 22]. Fig. 8 Theoretical variation of the pressure coefficient around the... Available from: https://www.researchgate.net/figure/Theoretical-variation-of-the-pressure-coefficient-around-the-cylinder-Strouhal-number_fig3_355844747

33. Batchelor, G. K. An Introduction to Fluid Dynamics. Cited in: Thermopedia. (n.d.). Tubes, Crossflow Over. Available at: https://www.thermopedia.com/content/1216/ [Accessed 22 Aug. 2025]. Cambridge: Cambridge University Press; 1970.

34. Mathworks. Patternsearch - Find minimum of function using pattern search - MATLAB [Internet]. [cited 2025 Aug 22]. Available from: https://se.mathworks.com/help/gads/patternsearch.html